Article

SOURCE DATA | TRANSPARENT PROCESS | OPEN ACCESS

EMBO reports

The structure of fly Teneurin-m reveals an asymmetric self-assembly that allows expansion into zippers

Jingxian Li[1,2,3,†], Sumit J. Bandekar[1,2,3,†] & Demet Araç[1,2,3,*]

Abstract

Teneurins are conserved cell adhesion molecules essential for embryogenesis and neural development in animals. Key to teneurin function is the ability of its extracellular region to form homophilic interactions in *cis* and/or in *trans*. However, our molecular understanding of teneurin homophilic interaction remains largely incomplete. Here, we showed that an extracellular fragment of Teneurin-m, the major teneurin homolog in flies, behaves as a homodimer in solution. The structure of Teneurin-m revealed that the transthyretin-related domain from one protomer and the β-propeller domain from the other mediates Teneurin-m self-association, which is abolished by point mutation of conserved residues. Strikingly, this architecture generates an asymmetric oligomerization interface that enables expansion of Teneurin-m into long zipper arrays reminiscent of protocadherins. An alternatively spliced site that exists only in vertebrates and regulates homophilic interaction in mammalian teneurins overlaps with the fly Teneurin-m self-association interface. Our work provides a molecular understanding of teneurin homophilic interaction and sheds light on its role in teneurin function throughout evolution.

Keywords adhesion; dimerization; Structural biology; synapse; teneurin
Subject Categories Cell Adhesion, Polarity & Cytoskeleton; Structural Biology
DOI 10.15252/embr.202256728 | Received 24 December 2022 | Revised 10 April 2023 | Accepted 12 April 2023
EMBO Reports (2023) e56728

Introduction

Cell-surface receptors mediate the recognition and adhesion between cells and initiate signaling to control countless developmental and regulatory processes. Teneurins (TENs) are critical cell-surface receptors conserved across metazoans and even in unicellular choanoflagellates (Tucker *et al*, 2012; Leamey & Sawatari, 2014; Mosca, 2015; Tucker, 2018; Baumgartner & Wides, 2019). *C. elegans* has one TEN homolog, Ten-1; *D. melanogaster* has two homologs, Ten-m and Ten-a, which are named for their major and accessory roles in the fly; vertebrates have four TEN homologs termed Ten1–Ten4 (Tucker, 2018).

TENs have multiple essential functions in animals that can be broadly categorized into functions in embryonic development and functions in the nervous system (Levine *et al*, 1994; Levine *et al*, 1997; Oohashi *et al*, 1999; Ben-Zur *et al*, 2000; Tucker *et al*, 2001; Fascetti & Baumgartner, 2002; Rubin *et al*, 2002; Zhou *et al*, 2003; Drabikowski *et al*, 2005; Tucker & Chiquet-Ehrismann, 2006; Broz *et al*, 2010; Tucker, 2018). During embryonic development, TENs are strongly expressed in the heart and the brain (Baumgartner *et al*, 1994; Levine *et al*, 1994; Tucker *et al*, 2001; Lossie *et al*, 2005; Tucker & Chiquet-Ehrismann, 2006; Nakamura *et al*, 2013). In flies, both the embryonic central nervous system and heart are severely malformed in the TEN-null embryo (Levine *et al*, 1994). TENs are essential for gastrulation and the epithelial to mesenchymal transition in mice (Ben-Zur *et al*, 2000; Zhou *et al*, 2003; Lossie *et al*, 2005; Nakamura *et al*, 2013); and for the correct germ cell development and formation of basement membranes in worms (Drabikowski *et al*, 2005; Trzebiatowska *et al*, 2008). During brain development, TENs guide axons to the correct targets (Drabikowski *et al*, 2005; Leamey *et al*, 2007; Dharmaratne *et al*, 2012; Hong *et al*, 2012; Mosca *et al*, 2012; Young *et al*, 2013) and regulate synapse formation (Leamey & Sawatari, 2014; Woelfle *et al*, 2016; Südhof, 2017). TEN perturbations cause synapse loss and impair synaptic organization *trans*-synaptically suggesting TENs act as bi-directional *trans*-cellular signaling molecules (Silva *et al*, 2011; Mosca *et al*, 2012; Boucard *et al*, 2014; Mosca, 2015). Mutations in TENs are linked to microphthalmia, congenital anosmia, and essential tremors and they are also associated with the progression of glioblastoma and ovarian cancer (Aldahmesh *et al*, 2012; Ziegler *et al*, 2012; Hor *et al*, 2015; Alkelai *et al*, 2016; Chassaing *et al*, 2016; Graumann *et al*, 2017; Talamillo *et al*, 2017).

TENs are large type-II transmembrane proteins (Jackson *et al*, 2018; Li *et al*, 2018; del Toro *et al*, 2020; Li *et al*, 2020; Meijer *et al*, 2022). From their N-termini, they have intracellular domains with putative nuclear localization sequences (Bagutti *et al*, 2003;

1 Department of Biochemistry and Molecular Biology, University of Chicago, Chicago, IL, USA
2 The University of Chicago Neuroscience Institute, University of Chicago, Chicago, IL, USA
3 Institute for Biophysical Dynamics, University of Chicago, Chicago, IL, USA
*Corresponding author. Tel: +1 7738342691; E-mail: arac@uchicago.edu
†These authors contributed equally to this work

Nunes *et al*, 2005). A single transmembrane helix is next, followed by the extracellular region (ECR) starting with eight epidermal growth factor (EGF) repeats which mediate a constitutive *cis*-dimer (EGF-dimer) through two disulfide bonds in EGF2 and EGF5 (Oohashi *et al*, 1999; Ben-Zur *et al*, 2000; Feng *et al*, 2002; Berns *et al*, 2018). Mature TEN molecules are composed of two TEN polypeptides linked in the EGF-dimer and presented on the extracellular surface. The TEN superfold (SF) follows the EGF repeats, where the remaining domains are organized around a large β-barrel (or YD-shell). A cysteine-rich domain (CRD) is followed by the transthyretin-related (TTR) domain which is alternatively spliced in flies. The Ig-like domain (or Fn-plug) is inserted inside the "bottom" of the barrel. Then a β-propeller domain (or NHL), which is alternatively spliced only in vertebrate TENs, packs against the β-barrel, Ig-like, and TTR domains (Berns *et al*, 2018; Li *et al*, 2018). Finally, there is a large β-barrel domain (or YD-shell; del Toro *et al*, 2020; Li *et al*, 2020), and a toxin-like domain (or ABD-Tox-GHH) which is partially inside the β-barrel. The two superfolds in a mature TEN molecule may be found freely moving in solution (Feng *et al*, 2002; Li *et al*, 2018), and they may also form dimers distinct from the EGF-dimer (Jackson *et al*, 2018; Li *et al*, 2020; Meijer *et al*, 2022).

TENs are reported to mediate their functions in a *trans*-cellular manner via the interaction of their large ECRs; this is suggested to occur either through *trans*-cellular homophilic interaction, or through their interaction with the latrophilin subfamily of adhesion G protein-coupled receptors (ADGRLs or LPHNs) (Berns *et al*, 2018; Li *et al*, 2020; Pederick *et al*, 2021; Zhang *et al*, 2022). *D. melanogaster* Ten-m is reported to direct olfactory synaptic partner matching as well as the formation of neuromuscular junctions (NMJs) through *trans*-cellular homophilic interactions (Hong *et al*, 2012; Mosca *et al*, 2012). In the mouse hippocampus, Ten3 has been suggested to instruct synapse specificity through homophilic *trans*-synaptic interactions (Berns *et al*, 2018; Pederick *et al*, 2021), whereas Ten2 mediates synapse specificity through heterophilic *trans*-synaptic interactions with a non-TEN ligand that is likely an ADGRL (Sando *et al*, 2019; Zhang *et al*, 2022). Using super-resolution microscopy, Ten3 was demonstrated to assemble into presynaptic nanoclusters of approximately 80 nm in most excitatory synapses of the hippocampus suggesting that TENs exist in oligomers that are larger in size than dimers (Zhang *et al*, 2022). Although the EGF-dimer and the heterophilic interaction of TEN with ADGRLs has been visualized via structural analysis (Feng *et al*, 2002; Li *et al*, 2018, 2020; del Toro *et al*, 2020), a molecular understanding of TEN self-association and whether TENs form *trans*- or *cis*- homophilic interactions (distinct from the constitutive EGF-dimer) remains unclear.

An alternatively spliced site in the β-propeller domain of mouse Ten3 is required to induce cell–cell aggregation via *trans* homophilic interaction (Berns *et al*, 2018), whereas the same splice site in human Ten2 diminishes the interaction of human Ten2 with ADGRL3 (Li *et al*, 2018). The presence of the splice site in human Ten2 induces inhibitory synapse formation in an artificial synapse formation assay (Li *et al*, 2018; Sando *et al*, 2019). The homodimer mediated by the spliced site was proposed to mediate a *cis* interaction (Li *et al*, 2020), whereas another study proposed a *trans* interaction (Jackson *et al*, 2018). Another proposed TEN dimer interface is mediated by the β-barrel and toxin-like domains although no mutagenesis experiments were performed to ensure this is indeed a biologically relevant dimerization interface (Meijer *et al*, 2022). *Trans*-cellular interaction of Ten-m has been reported (Hong *et al*, 2012; Mosca *et al*, 2012), but current studies are limited by a lack of mechanistic detail, for instance, whether Ten-m performs its function through direct interactions or whether it requires another ligand to mediate *trans* interactions.

Herein we studied the homophilic self-association of Teneurin-m, the major TEN homolog in fruit flies. We used gel filtration chromatography to show that Ten-m behaves as a homodimer in solution in a concentration-dependent manner. The 2.4 Å crystal structure of Ten-m revealed a large self-association interface mediated by the transthyretin-related domain from one protomer and β-propeller domain from the other. This organization generates an asymmetric interface which allows for the addition of incoming protomers to create long zipper arrays reminiscent of protocadherins; these zippers are consistent with the observation of the large Ten3 nanoclusters *in vivo* (Zhang *et al*, 2022). Point mutations in conserved residues at the interface abolished observed Ten-m dimer formation. A vertebrate-only alternatively spliced site in the β-propeller domain which regulates homodimerization and ADGRL binding in mammalian TENs overlaps with the Ten-m self-association interface, suggesting that this splice site might have evolved to finely regulate homophilic interactions. Evaluation of our Ten-m structure reveals that the self-association interface is compatible with both *cis*- and *trans*-association of Ten-m. Our work provides molecular-level evidence that Ten-m can directly oligomerize, and we provide important point mutations which will help understand the role of homophilic interaction in Tem-m function.

Results

The Teneurin-m superfold self-associates in solution and has similar structure to vertebrate TENs

We purified the Ten-m superfold (Ten-m^{SF}) containing residues 779–2731, including the CRD through the toxin-like domain (Fig 1A). While purifying the construct, we observed that the elution volume of Ten-m^{SF} on size exclusion chromatography (SEC) was consistent with a dimer in a concentration-dependent manner (Fig 1B). The equivalent human Ten2 (hTen2) construct displays only a small shift in elution volume (Fig 1C). We used selenomethionine labeling to determine the crystal structure of *D. melanogaster* Ten-m^{SF} to 2.4 Å resolution (Fig 1D and Table 1) and found that it was structurally homologous to vertebrate TENs (Fig 1E; Meijer *et al*, 2022). Our Ten-m structure retains the major structural features of vertebrate TEN structures, with a few differences. The N-terminus of the CRD is not resolved, and the toxin-like domain has the C-terminal portion unresolved (Figs 1D and EV1A). Minor structural differences are also present, such as the tracks of the Ig-like (Fig EV1B) and toxin-like domains (Fig EV1C) inside the β-barrel. When ADGRL binding is modeled using the structure of the hTEN2:hADGRL3 complex (PDB 6VHH), a β-strand protruding from the β-barrel sterically clashes with the lectin domain of hADGRL3 (Fig EV1D). Compared to human Ten2 (PDB 6VHH), an alignment of the Ten-m structure produces an all-atom RMSD of 5.7 Å; a

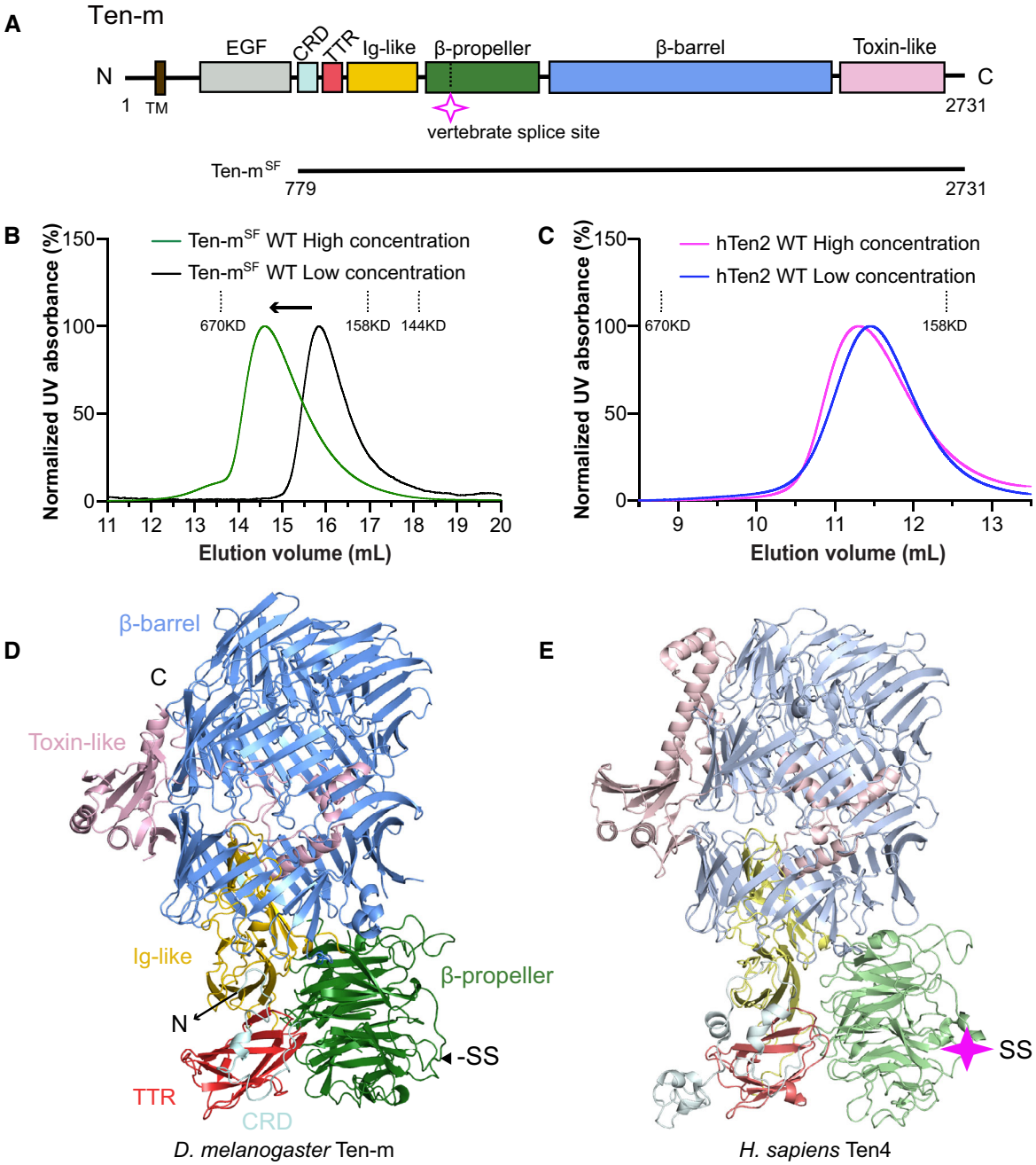

Figure 1. Ten-m behaves as a concentration-dependent dimer in solution and has a similar fold to vertebrate TENs.

A Domain architecture diagram of Ten-m with domains shown as rectangles. TM, transmembrane domain; EGF, epidermal growth factor repeats; CRD, cysteine-rich domain; TTR, transthyretin-related domain; Ig-like, immunoglobulin-like domain. A horizontal solid black line below the diagram shows the domain boundary of the construct used in this study, the Ten-m superfold (Ten-m^{SF}), with the position of the vertebrate-only splice site shown as an open pink star.

B Size exclusion chromatograms of Ten-m^{SF} at low concentration (0.01 mg/ml, black curve) and high concentration (0.63 mg/ml, green curve) show a shift in elution volume in agreement with formation of a dimer species at high concentration, normalized A_{280} plotted vs. elution volume. The elution volumes of gel filtration chromatography standards are indicated on the figure with vertical dashed lines. SEC experiments were performed once, $N = 1$.

C Gel filtration chromatograms of hTen2 at low concentration (blue) and high concentration (pink). A large shift is not observed with hTen2. The elution volumes of protein standards are shown as in B.

D, E A structural comparison of the Ten-m^{SF} crystal structure with the most complete vertebrate TEN structure to date, Ten4^{SF} (PDB 7BAM) shows that the folds of invertebrate and vertebrate TENs are structurally homologous. A filled pink star shows the location of the vertebrate-specific splice insert in the β-propeller domain and the equivalent location is marked on Ten-m structure as (-SS).

Source data are available online for this figure.

Table 1. Data collection and refinement statistics.

	Ten-m A_{Native}	Ten-m A_{SeMet}
Wavelength (Å)	1.033	0.9792
Resolution range (Å)	47.6–2.4 (2.486–2.4)	65.33–2.95 (3.055–2.95)
Space group	$P2_12_12_1$	$P2_12_12_1$
Unit cell dimensions (Å)	95.203 129.857 188.158	95.189 130.76 187.79
Total reflections	628,823 (61532)	344,116 (35290)
Unique reflections	91,702 (9032)	50,034 (4923)
Multiplicity	6.9 (6.8)	6.9 (7.2)
Completeness (%)	99.90 (99.97)	99.69 (99.66)
Mean I/σI	10.09 (1.00)	9.49 (1.87)
Wilson B-factor	53.88	54.58
R-merge	0.1438 (1.533)	0.2735 (1.367)
R-meas	0.1558 (1.66)	0.2965 (1.473)
R-pim	0.05937 (0.6307)	0.113 (0.546)
$CC_{1/2}$	0.996 (0.537)	0.981 (0.667)
CC*	0.999 (0.836)	0.995 (0.894)
Reflections used in refinement	91,686 (9031)	
Reflections used for R-free	1,697 (168)	
R-work	0.2183 (0.3503)	
R-free	0.2417 (0.3862)	
$CC_{(work)}$	0.948 (0.681)	
$CC_{(free)}$	0.928 (0.640)	
Number of non-hydrogen atoms	14,844	
Macromolecules	14,201	
Ligands	334	
Solvent	309	
Protein residues	1772	
RMS bonds (Å)	0.009	
RMS angles (°)	1.26	
Ramachandran favored (%)	95.14	
Ramachandran allowed (%)	4.64	
Ramachandran outliers (%)	0.29	
Rotamer outliers (%)	1.55	
MolProbity Clashscore	5.15	
Average B-factor	68.53	
Macromolecules	68.30	
Ligands	92.00	
Solvent	53.86	
Number of TLS groups	9	

Statistics for the highest-resolution shell are shown in parentheses.

5.9 Å RMSD compared to human Ten4 (PDB 7BAM); a 5.8 Å RMSD when compared to chicken Ten2 (PDB 6FB3), and a 5.1 Å RMSD compared to mouse Ten3 (PDB 6FAY) (Fig EV1E). In contrast, deposited vertebrate TEN structures are within 3.1 Å RMSD of each other. The lower structural homology goes hand in hand with lower sequence homology; Ten-m retains 35% sequence identity in comparison to vertebrate TENs, whereas vertebrate homologs have at least 75% sequence identity (Fig EV1F). The sequence identity of Ten-m compared to vertebrate TENs varies by domain and decreases from the N-terminus to the C-terminus: the TTR domain has 50% identity, whereas the toxin-like domain only retains 25% identity (Fig EV1G–K).

The Ten-m crystal structure reveals an asymmetric self-association interface that allows expansion into longer multimers

The Ten-m crystal structure contained only one copy of the protein in the asymmetric unit, so we searched if the observed dimer in solution could be represented by any of the crystal packing interfaces. We found one packing interface which buries a large amount of surface area from solvent at 2700 $Å^2$ and is primarily composed of hydrophobic residues, both indicators of protein–protein interfaces. This interface is formed by the TTR domain of one Ten-m monomer interacting with the β-propeller domain of the next monomer to create a structure with dimensions 180 × 140 × 60 Å (Fig 2). In the TTR/β-propeller interface, the face of TTR farthest from the β-barrel on the same monomer interacts with the open face of the β-propeller on another monomer, sandwiching one monomer's β-propeller between two TTR copies, albeit different surfaces (Fig 2A–C). Another small portion of the interface includes the β-propeller from one protomer interacting with the β-propeller of another protomer. We examined other packing interfaces using ePISA (Krissinel & Henrick, 2007), but they bury far less surface area at 420 $Å^2$ and 150 $Å^2$ and they are poorly conserved, so we did not pursue them (Appendix Fig S1A and B).

The asymmetric nature of the Ten-m self-association interface leaves each interaction surface open for interaction with another protomer (Fig 3A), allowing for repetition into longer multimers. Our crystal packing is consistent with this idea as the interface falls exactly along one of the crystallographic $P2_1$ screw axes (Fig 3B); each monomer is related to the next one by a translation of 48 Å and a rotation of 180°. Ten-m oligomers can be built *ad infinitum* in this manner. We see shoulders in our SEC curves that contain Ten-m by SDS-PAGE; this is consistent with the presence of a small amount of higher-order Ten-m species (Fig 3C). Our mass photometry data are also consistent with the presence of higher-order Ten-m species at higher concentrations (Fig EV2). At low concentrations, we see populations of monomer (~ 222 kD) and dimer (~ 444 kD) (Fig EV2A). At high concentrations (Fig EV2B and C) we see a larger spread in our data. The curve is centered around a dimer species by molecular mass, but the low end of the curve corresponds with our monomer, and the high end of the spread includes masses which are consistent with the trimer at ~ 666 kD and tetramer at ~ 888 kD. This is consistent with an equilibrium from at least monomer to roughly tetramer present in solution.

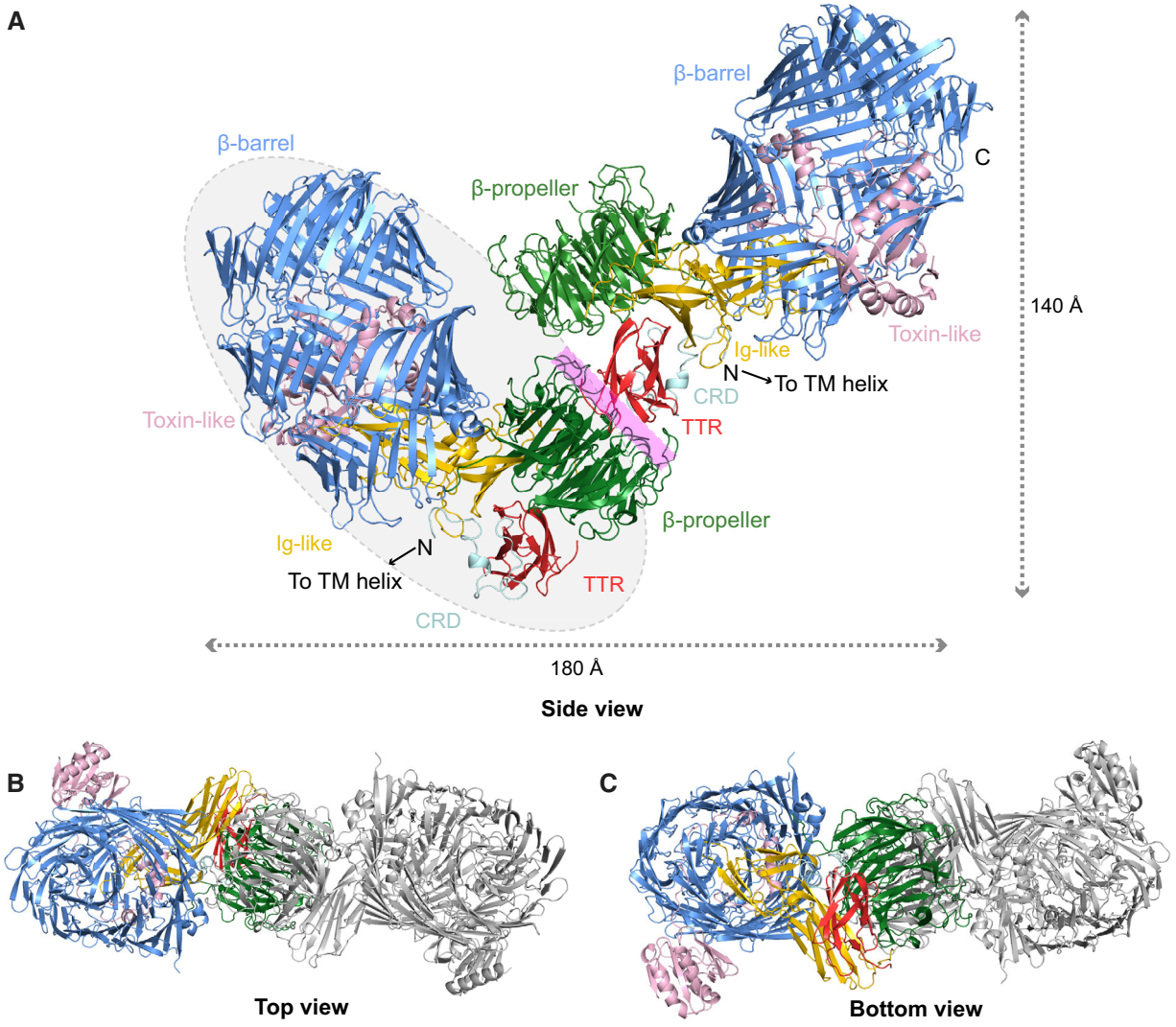

Figure 2. Ten-m structure reveals an asymmetric self-association interface.

A The proposed Ten-m self-association interface is shown in cartoon representation, which is composed of the β-propeller in one monomer (green) interacting with the TTR (red) and β-propeller (green) of another monomer. The left monomer is outlined with a dotted oval, and the interface is shown with a solid pink bar. N- and C- termini are labeled when visible. Dotted lines show the approximate dimensions of a dimer structure.

B, C Top and bottom views of the dimer show the antiparallel nature of the Ten-m self-association interface.

Source data are available online for this figure.

The Ten-m self-association surface is a broad surface primarily composed of hydrophobic residues

Our proposed Ten-m self-association interface (Fig 4A) buries 2,700 Å^2 from solvent (Fig 4B) and employs greater than 80 residues. We employed the ConSurf server to check whether our TTR/β-propeller interface was conserved throughout evolution (Ashkenazy *et al*, 2016). We found that the entire surface area of the interface (Fig EV3A) was well conserved within arthropods. Due to its large extent, here we divide up the interface into three patches and highlight important interactions (Fig 4C). Patch 1 contains the small number of interactions that occur between adjacent β-propeller domains (Fig 4D), with R1312 and D1313 of one monomer making salt bridges with E1454 and R1427 of the next monomer. S922 of the TTR domain also interacts with Q1426 of the next protomer's β-propeller. Patch 2 (Fig 4E) also has some hydrophilic interactions, with Y1494 of the β-propeller forming a network of interactions including the backbone carbonyls of P917, R919, and M942 on the TTR domain. The side chain of R919 makes another interaction with the backbone of A1492 and the backbone carbonyl of M942 interacts with Q1156. A hydrophobic cleft also exists in patch two, where P917 and M942 from the TTR domain nestle against L1174, A1175, V1177, F1192, and Y1494. Patch 3 (Fig 4F) is dominated by hydrophobic interactions: W1347 is supported on its protomer's β-propeller by Y1287 and is cradled by three residues on the opposing TTR domain, L847, Y850, and

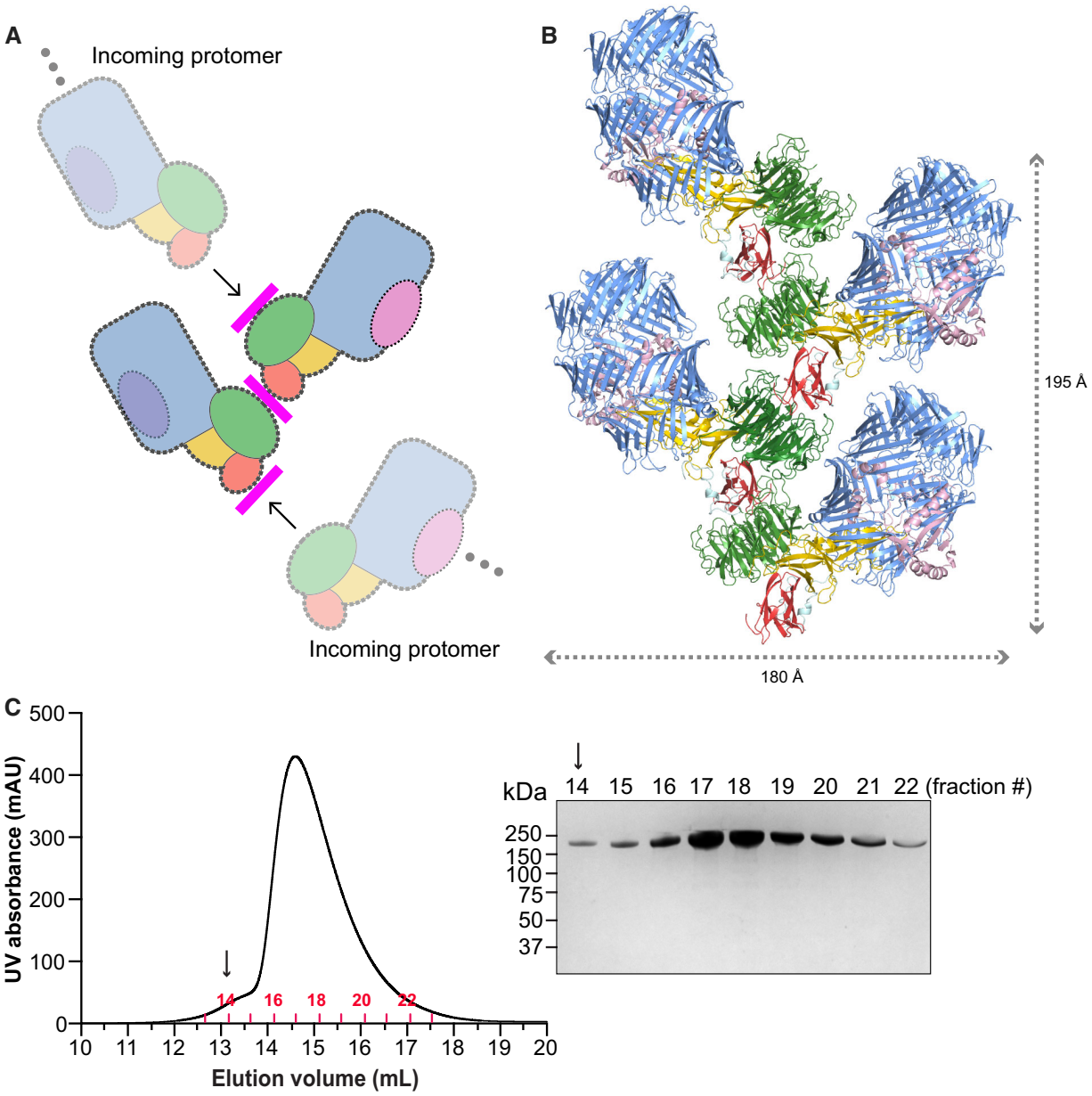

Figure 3. The asymmetry of the Ten-m self-association interface allows for repetition into longer multimers.

A The observed Ten-m dimer from SEC is shown in bright colors and each monomer is enclosed by a dotted line. The interface is shown as bright pink bars between each monomer. Unoccupied surfaces on the TTR (red) and β-propeller (green) can accommodate more protomers to extend the interface into a longer multimer.

B The Ten-m self-association interface coincides with one of the $P2_1$ screw axes in the crystal, supporting the idea that the interface can extend into larger multimers. Four copies of Ten-m are shown in cartoon representation along the mentioned axis to demonstrate how a Ten-m oligomer would appear.

C Size exclusion chromatogram with A_{280} plotted versus elution volume and accompanying reducing SDS-PAGE stained with Coomassie Brilliant Blue shows that the shoulder at the front of the SEC peak (fraction 14, arrow) contains Ten-m and is consistent with higher order species in solution.

Source data are available online for this figure.

F890. V877 opposes V1215, and Y850 makes a hydrogen bond with the backbone carbonyl of C1266.

Since the TTR/β-propeller interface contains some hydrophilic and hydrophobic residues, we tested the NaCl dependence of Ten-m self-association using size exclusion chromatography (Fig EV2D). We found that higher salt concentrations at a constant protein concentration caused the protein to shift toward the observed dimer elution volume. In addition, the shoulder of the Ten-m peak, which may correspond to a higher-order species of Ten-m, has higher absorbance in the higher salt concentration conditions.

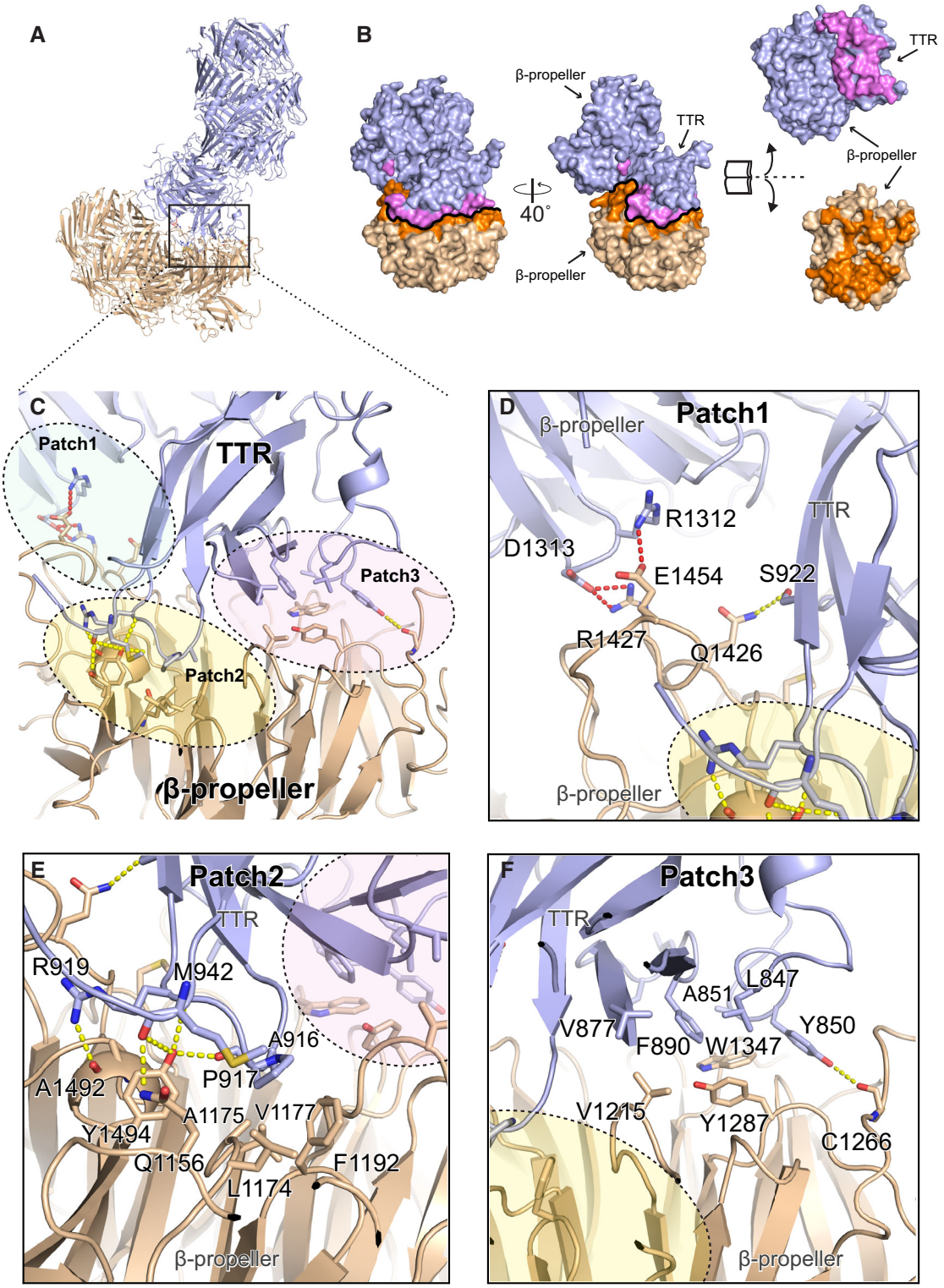

Figure 4.

Ten-m self-association can be abrogated in solution by point mutation of conserved residues

To validate the proposed Ten-m self-association interface, we generated point mutations in key residues found on the β-propeller domain which contact multiple residues and bury a large amount of surface area from solvent (Fig 5A). We started with three residues due to the large number of contacts they make and their high sequence conservation (Figs 4E and F, and EV3B): F1192, Y1287, and W1347. Using a quadruple mutant including F1192A, Y1287A,

Figure 4. The Ten-m self-association interface is large and is mediated by hydrophobic residues.

A The overall structure of Ten-m self-association is shown using a cartoon representation of two monomers, one wheat and another purple.

B Two monomers in surface representation, with only the domains involved in the interface used, illustrates the total surface area of 2,700 Å^2 that the interface covers, with a closed and open book view shown. Pink and orange colors are used to highlight portions of the surface involved in the interface.

C A zoomed in view of the interface in A with individual residues shown as sticks. The surface is broad and is divided into three patches, each highlighted with a colored oval.

D–F Patches 1, 2, and 3 are shown in detail, with individual residues shown as sticks, with salt bridges shown as red dotted lines, and hydrogen bonds shown in yellow dotted lines. Patch 1 is comprised of salt bridges and a hydrogen bond, whereas patches 2 and 3 are mostly hydrophobic, with a few hydrogen bonds.

Source data are available online for this figure.

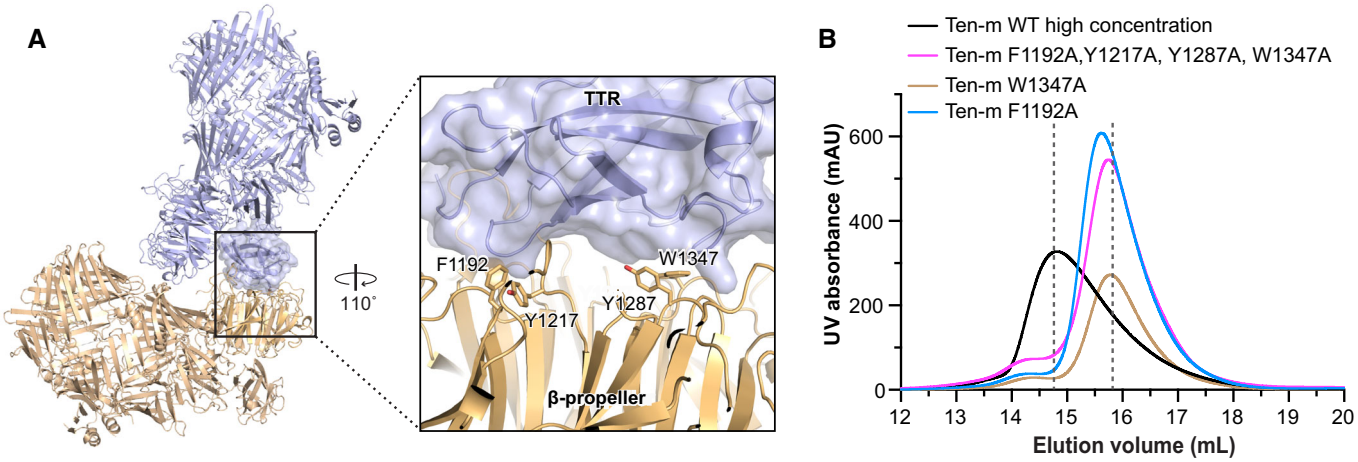

Figure 5. Structure-guided point mutations disrupt Ten-m self-association in solution.

A The Ten-m self-association interface is shown in a cartoon representation, with the TTR domain of one monomer in purple, and the β-propeller of another copy shown in wheat. Key aromatic residues in the β-propeller that bury a large amount of surface area against the TTR domain and make several contacts are shown as sticks and labeled.

B Size exclusion chromatograms with A_{280} values plotted versus elution volume show that the introduction of alanine residues in place of important aromatic residues (W1347A, wheat, F1192A, Blue, or a quadruple mutant of F1192A, Y1217A, Y1287A, and W1347A, pink) run at a later elution volume than wild-type Ten-m (black), suggesting that despite a similar or higher peak concentration, these proteins are monomeric in solution. Vertical dotted lines show the expected position of the dimer around 14.6 ml and the monomer at 15.8 ml. SEC experiments were performed once, $N = 1$.

Source data are available online for this figure.

W1347A, and Y1217A, (Y1217A was changed mistakenly), we found that even at high concentrations, this mutant eluted as an apparent monomer in SEC (Fig 5B). Single point mutations of W1347A and F1192A were also able to shift the SEC peak of Ten-m from dimer toward monomer (Fig 5B), suggesting that the hydrophobic residues in patches 2 and 3 are key for stabilizing the Ten-m interface in solution. We also tested whether the insertion of a 9-residue alternatively spliced sequence present in arthropod TENs had the ability to affect Ten-m self-association. The splice insert is hydrophobic in character (SIFWNYFNA) and is found in the TTR domain, near the interface yet faced away from it (Appendix Fig S2A). We found that the presence of the splice insert did not disrupt observed dimer formation (Appendix Fig S2B).

An alternatively spliced site in vertebrates overlaps with the fly self-association interface

When the vertebrate TEN β-propeller domain containing the vertebrate splice insert (RNKDFRH) is superimposed with the Ten-m self-association interface, a steric clash is observed between the two (Fig 6A). Moreover, the vertebrate splice sequence directly overlaps in three-dimensional space with our identified patch 2 (Fig 6B), specifically with F1192, a conserved residue in the Ten-m interface which disrupts the observed dimer when mutated. This implies that the presence of this spliced sequence is not compatible with the TTR/β-propeller interface shown here, and this further suggests that the splice site may have evolved to regulate interactions on this patch.

Discussion

TENs are critical cell adhesion molecules conserved across animals (Tucker *et al*, 2007, 2012; Tucker, 2018). The homophilic interactions of TENs have been implicated in the processes of neuronal wiring in both invertebrates and vertebrates (Hong *et al*, 2012; Mosca *et al*, 2012; Mosca & Luo, 2014; Berns *et al*, 2018; Pederick *et al*, 2021; Zhang *et al*, 2022). In this work, we determined the high-resolution crystal structure of Ten-m, revealed its self-association interface, and identified point mutations that break the observed dimer on SEC.

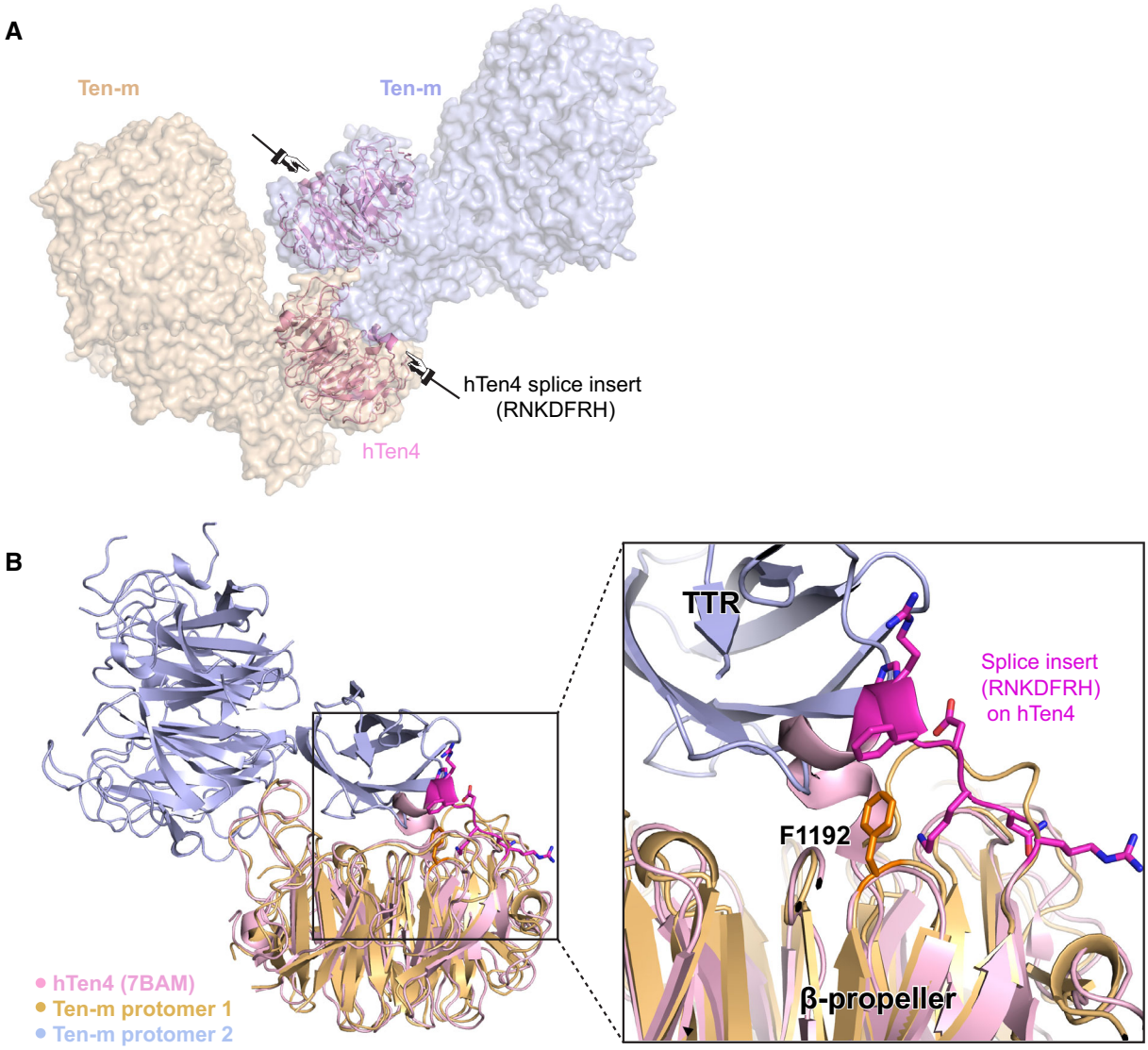

Figure 6. The vertebrate-specific splice insert in the β-propeller domain overlaps with Patch 2 of the Ten-m self-association surface.

A The Ten-m self-association interface is shown using two individual monomers shown in wheat and purple in surface representation. In cartoon representation, colored pink, is hTen4 containing the vertebrate +SS aligned by the β-propeller domain. An arrow points out the location of the spliced sequence.

B Structural superimposition of β-propeller domains from Ten-m (colored as above) and hTen4 (pink) shows that F1192 is in close proximity to the vertebrate +SS (shown in bright pink with side chains shown as sticks).

Source data are available online for this figure.

Ten-m may use the TTR/β-propeller interface to expand into zippers on cell surfaces

The Ten-m self-association interface is mediated by two different Ten-m domains from each protomer, creating an asymmetric interface (Fig 2) and leaving each protomer with an open interface available for a new incoming protomer (Fig 3A). The asymmetric nature of the Ten-m self-association surface means that it has the potential to accept an infinite number of new protomers and form long multimer structures or "zippers" (Fig 7) reminiscent of protocadherins (Brasch *et al*, 2019). Protocadherins are alternatively spliced cell-surface receptors that form zippers between nerve cells using a combination of isoform-promiscuous *cis* dimers and isoform-specific homophilic *trans* dimers; these zippers signal to avoid a nerve cell from making a synapse onto itself (Thu *et al*, 2014; Goodman *et al*, 2016; Brasch *et al*, 2019). Similar to protocadherins, we speculate that Ten-m zippers might be used to specify self in the process of neural wiring. Consistent with the presence of higher-order species, we observe shoulders on our SEC peaks which contain Ten-m by SDS-PAGE (Fig 3C) and we also observe higher order species in mass photometry at high concentrations (Fig EV2B and C). Furthermore, the crystal packing of this structure revealed the architecture of such a zipper (Fig 3B).

A recent report that imaged mouse hippocampal neurons using super-resolution microscopy showed that TENs can form 80 nm

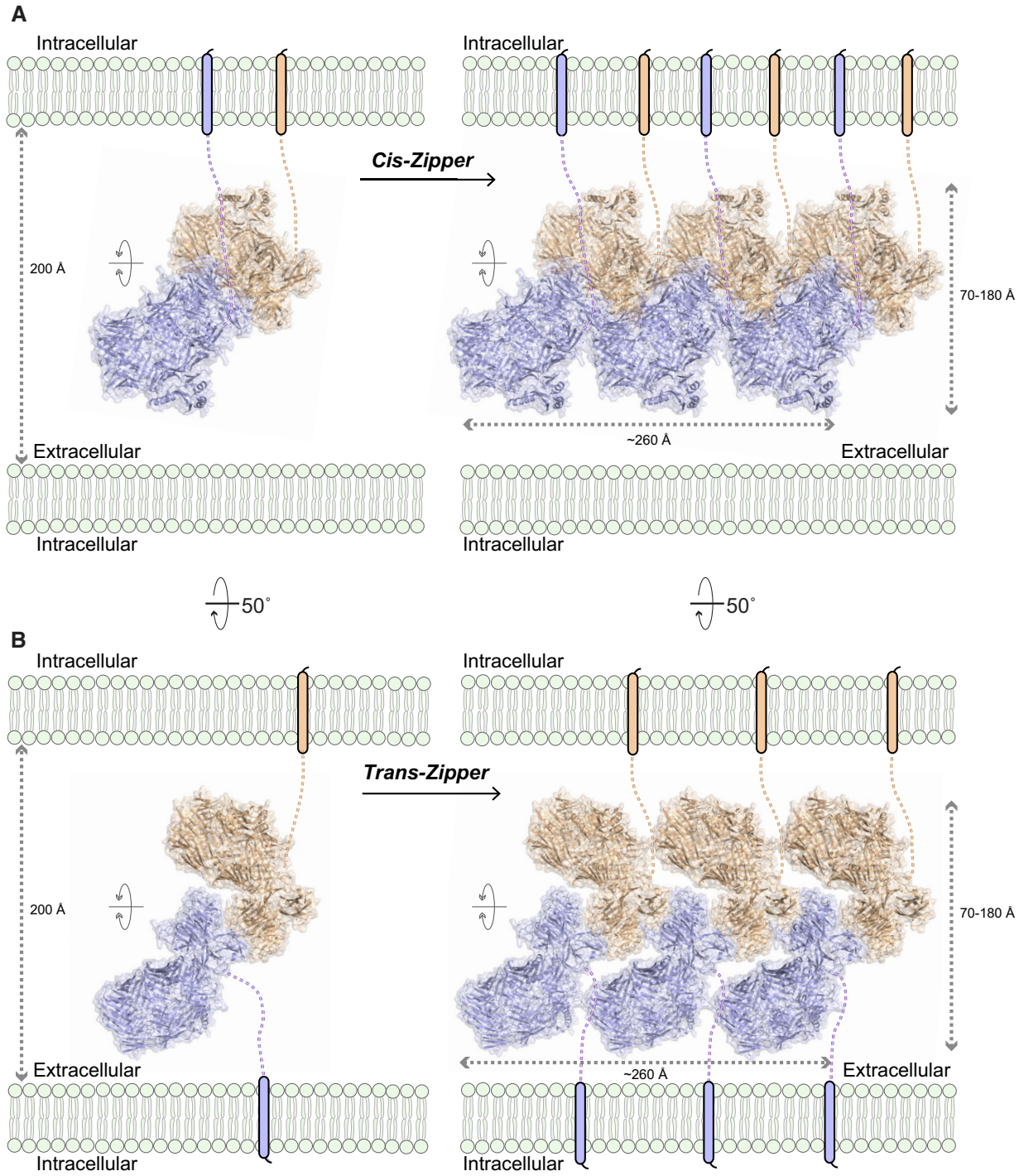

Figure 7. Models for Ten-m self-association and zipper formation.

A, B The Ten-m self-association interface identified in this work is compatible with both a *cis* interaction mode, (A) and a *trans* interaction mode, (B) each allowing for repetition into zipper structures (right). Two opposing cell membranes are shown with TEN molecules projecting out of them, with intracellular faces toward the top and bottom of the page, and an extracellular space in the middle of the page. TEN superfolds are shown as a cartoon representation, linked to their transmembrane helices (shown as rounded cylinders) by dotted lines representing the EGF repeats. Please also see Fig EV4 for details including how constitutive *cis*-dimerization via the EGF repeats fits into the models.

(800 Å) nanoclusters in the synaptic cleft equally distant from pre- and post-synaptic markers (Zhang *et al*, 2022). A nanocluster of 800 Å can accommodate 10–15 Ten-m monomers within a Ten-m zipper, consistent with the idea that Ten-m may form higher order structures on cell surfaces. Other recent reports show that TENs are key in synaptic organization, which requires precise distance

restraints that could be imposed by the TEN zipper (Mosca *et al*, 2012; Mosca & Luo, 2014; Mosca, 2015). This may be only a part of the picture, where the kinetics of zipper formation and disassembly are dynamically regulated by other protein binding partners, such as ADGRLs, and the overall environment of the TEN-presenting cell.

Teneurin-m self-association is compatible with both *cis*- and *trans*- orientation

Our results show that Ten-m behaves as a dimer in solution in the context of the Ten-m^{SF} construct, which lacks the transmembrane helix and EGF repeats that mediate the constitutive EGF-dimer of TENs. If we assume these EGF repeats are extended, our TTR/β-propeller interface is compatible with both *cis* (Fig 7A) or *trans* (Fig 7B) modes of interaction in the context of full-length TEN. Moreover, many possibilities exist to describe how the TTR/β-propeller interface forms in relation to the EGF-dimer of the mature TEN molecule (Fig EV4A and B).

Nevertheless, we show the TTR/β-propeller-mediated Ten-m oligomer exists in solution as an abundant species rather than representing a small fraction of the species because point mutations at this interface strongly reduce the amount of the dimer species in our size exclusion chromatograms (Fig 5).

Conservation of self-association surfaces between vertebrates and invertebrates

Vertebrate TENs are thought to use a seven-residue β-propeller splice insert to regulate dimerization where the presence of the splice insert favors dimerization (Berns *et al*, 2018; Li *et al*, 2020). In comparison, Ten-m is not alternatively spliced at this site and has the shorter sequence. Strikingly, superimposition of the vertebrate TEN structures with the fly Ten-m reveals that the β-propeller splice insert lays directly on top of patch 2 residues that are critical for Ten-m self-association, most notably F1192 (Fig 6). The residues at the Ten-m interface are conserved among arthropods (Fig EV3A), but not strongly conserved outside of this phylum (Fig EV3C). This may represent an evolutionary divergence with how dimerization is regulated in different TEN orthologs. In addition, the Ten4 dimer surface is not conserved in arthropods (Fig EV3D). Ten-m self-association is not regulated by alternative splicing (Appendix Fig S2) and uses the TTR/β-propeller interface we describe in this manuscript (Fig 2). In contrast, we speculate that vertebrates evolved the β-propeller splice site as a method to tightly regulate TEN self-association and ADGRL interaction (Li *et al*, 2020), thus allowing for increased functional complexity and diversity.

Other TEN self-association interfaces and modes of homophilic interaction

Several dimer interfaces have been reported for mammalian TENs. The Ten-m self-association interface differs from other TEN dimers in that it is asymmetric and thus allows for repetition into higher order species (Figs 7 and EV5A). In contrast, the Ten4 dimer (Meijer *et al*, 2022) determined by cryoEM is symmetric about an interface formed by the β-barrel and toxin-like domains (Fig EV5B), and the dimer structure proposed for Ten2 (Jackson *et al*, 2018; Li *et al*, 2020) is symmetric with respect to the vertebrate-only β-propeller splice insert (Fig EV5C) (Jackson *et al*, 2018). Other groups have presented structurally sound models for TEN self-association (Jackson *et al*, 2018; Meijer *et al*, 2022), yet no mutagenesis studies were performed to rigorously validate their models.

Our structurally validated model for Ten-m self-association provides a new framework for understanding this complex and extremely relevant process. Future exciting work will use the single point mutations we provide here to understand how Ten-m oligomerization fits in to the complexities of nervous system development.

Materials and Methods

Cell culture

As previously described (Li *et al*, 2020), High Five insect cells (*Trichoplusia ni*, female, ovarian. ThermoFisher, B85502) were used for production of recombinant proteins. Cells were cultured using Insect-Xpress medium (Lonza, 04351Q) with 10 μg/ml gentamicin at 27°C.

Cloning and construct design

Similar to previously described (Li *et al*, 2020), *D. melanogaster* Ten-m (UniProt entry O61307-1, Ten-m isoform B) was inserted into the pAcGP67a vector. Sf9 cells (Thermo Fisher, 12659017) were transfected with Ten-m plasmids and commercial baculovirus DNA (Expression Systems, 91–002) using Cellfectin II (Thermo Fisher, 10362100). High-titer recombinant baculovirus was obtained using Sf9 cells grown in SF900-III medium with 10% (v/v) FBS (Sigma-Aldrich, F0926). High Five cells (Thermo Fisher, B85502) were infected with baculovirus at 2.0×10^6 cells/ml and incubated at 27°C with 120 rpm shaking for 72 h. Ten-m^{SF} (residues L779-A2731) was cloned with a 6x polyhistidine tag at the C-terminus. Ten-m^{SF} was amplified using these primers: F: 5′-CGCATTCTG CCTTTGCGGCGGATCCCTTGAACTGTGGCGACAGCAAG-3′ and R: 5′-GAAAGGATCAGATCTGCAGCTTAGTGATGGTGATGGTGATGCG CACTCAGCTCGCCGAAC-3′. Ten-m F1192A primers were F: gcagt cttttcgtcggtgatgctaattacatccgccgcatc and R: gatgcggcggatgtaattagcat caccgacgaaaagactgc. Ten-m Y1217A primers were F: cgcgtctcgGC ccgctaccacatggcccand R: atgtggtagcgggccgagacgcgagtcgcgtt. Ten-m Y1287A primers were F: caaaggatgccaaattggctgctccgaaaggcattgcga tttc R: gaaatcgcaatgcctttcggagcagccaatttggcatcctttg. Ten-m W1347A primers were F: ggagatgcatcttcgcgcgcccactgagctagcagt R: tgctagctca gtgggcgcgcgaagatgcatctcct.

Protein expression and purification

As previously described (Li *et al*, 2020), media were harvested from cell cultures 72 h after infection. The media were centrifuged at room temperature at 900 *g* for 15 min. The supernatant was harvested and transferred to a beaker with stirring at room temperature and the following were added: 50 mM Tris pH 8.0, 5 mM $CaCl_2$, and 1 mM $NiCl_2$ (final concentrations listed). After 30 min, the solution was centrifuged for 30 min at 8,000 *g*. The clarified

supernatant was then incubated with nickel-nitriloacetic (Ni-NTA) resin (QIAGEN 30250) with stirring at room temperature for 3 h. A Büchner funnel was used to collect resin and wash using a buffer composed of 10 mM HEPES pH 7.2, 150 mM NaCl (HBS), and 20 mM imidazole, and then the washed resin was transferred to a poly-prep chromatography column (Bio-Rad). The protein was eluted using HBS buffer containing 200 mM imidazole. Fractions containing desired protein were pooled and concentrated using a 100 kDa centrifugal concentrator (Amicon UFC810024) and loaded on gel-filtration chromatography using a Superose 6 Increase 10/300 column (GE Healthcare) and the following buffer: 25 mM Tris pH 8.0, 150 mM NaCl. Selenomethione-labeled Ten-m^{SF} was expressed as previously described (Dong *et al*, 2009; Leon *et al*, 2020). High Five cells were grown in ESF921 medium (Expression Systems, 96-001-01). Cells were then centrifuged at 100 *g* for 15 min and resuspended in methionine-free ESF921 medium (Expression Systems, 96–200). Cells were infected using Ten-m recombinant baculovirus at a density of 2.0×10^6 cells/ml. Ten hours after infection, 100 mg seleno-L-methionine (Sigma–Aldrich, S3132) per liter of culture was added. An additional 150 mg seleno-L-methionine was added to each liter of cell culture at 36 h post-infection. The cells were harvested 72 h post-infection and the purification process was the same as described above.

Protein crystallography

Purified Ten-m^{SF} was concentrated to 8.8 mg/ml using a 100 kDa cutoff centrifugal concentrator system (Amicon UFC810024) and applied to sitting drop crystal trays in a drop volume of 0.2 µl against a well volume of 50 µl. Crystals were grown in a well solution consisting of 0.5 M ammonium sulfate with 16% PEG 3350. Crystals grew at room temperature and appeared after 7 days. Crystals were looped from their mother liquor and transferred to a cryoprotection solution of original mother liquor supplemented with 30% glycerol and then immediately frozen in liquid nitrogen. SeMet crystals were grown and harvested under the same conditions.

X-ray data collection, reduction, and analysis

Frozen crystals were shipped on liquid nitrogen to the GM/CA beamline or the NE-CAT beamline at the Advanced Photon Source at Argonne National Labs for remote data collection at 110 K. Two datasets were collected in P_{212121}, crystal form A_{Native} and its SeMet derivative A_{SeMet}. The final resolution was determined using shells which contain $CC_{1/2} > 0.5$ using analysis done by aimless. Detailed data collection and processing statistics are available in Table 1. Data collected at GM/CA were reduced, indexed, integrated, and scaled using the automated data processing suites of GM/CA (AutoPROC) which employs XDS and aimless. Data collected at NE-CAT were similarly processed but using their automatic data processing workflow called RAPD.

Structure solution and model building

All structural solution and model building phases were carried out using the PHENIX suite of software for macromolecular crystallography (Liebschner *et al*, 2019). A partial solution was first obtained with A_{Native} using molecular replacement in PHASER (McCoy *et al*, 2007) of the Ig-like and β-propeller domains of chicken Ten2 (PDB 6FB3). Using this original model (or other published structures) to determine or manually build the rest of the Ten-m structure was not successful and thus we switched to SeMet techniques. Using the partial model from molecular replacement and SeMet-SAD, we obtained an experimentally phased density map using the MR-SAD module in PHASER. This density map was density modified using RESOLVE (Terwilliger, 2003) and used to manually build the structure using Coot (Emsley *et al*, 2010), using PDB 6FB3 as a guide to place secondary structure elements. During the manual building process, AlphaFold was released to the public via ColabFold and we used ColabFold (Mirdita *et al*, 2022) generated models of Ten-m to further guide manual building. Following extensive manual building using the density-modified maps from A_{SeMet}, we used molecular replacement to move our manually built model into the native crystal form A_{Native}, and switched to refinement against A_{Native} using phenix.refine (Liebschner *et al*, 2019). Initial rounds of refinement used alternating rounds of real and reciprocal space refinement using individual B-factors. Next rounds of refinement included the previous parameters but also included translation-libration-screw refinement, optimization of X-ray/stereochemistry weight, and optimization of X-ray/ADP weight. Final rounds of refinement included individual B-factor refinement, translation-libration-screw refinement, optimization of X-ray/stereochemistry weight, and optimization of X-ray/ADP weight, and rigid body refinement. The model based on crystal form A_{Native} was finalized using Coot's built-in validation tools including MolProbity (Williams *et al*, 2018).

Structural analysis and sequence conservation analysis

Structural analysis and manual inspection of structures were performed using PyMOL version 2.4.1 (Schrodinger) and sequence analysis was done using PROMALS3D (Pei *et al*, 2008) and the ConSurf (Ashkenazy *et al*, 2016) server. The align function in PyMOL was used to generate root mean squared deviation (RMSD) values between TEN structures.

Analytical size exclusion chromatography

Standards were run in buffer comprised of 25 mM Tris pH 8.0, 150 mM NaCl on a Superose 6 column for direct comparison. Ten-m wild type and variants were prepared in the same buffer, concentrated using a 100 kDa cutoff centrifugal concentrator system (Amicon UFC810024), and filtered through 0.22 µm filters and run using the above buffer, supplemented with additional NaCl as necessary.

Mass photometry

Mass photometry experiments were performed in the Biophysics core facility on a Refeyn Two^{MP} at the University of Illinois-Chicago. The instrument was calibrated using β-Amylase and thyroglobulin. First, Ten-m samples were purified as described above, and samples were diluted in SEC buffer to various concentrations from 10 nM to 500 nM. 3,000 frame movies were collected and individual counts were recorded, and masses were extrapolated using calibration curves. The data were examined and plotted using Refeyn DiscoverMP software.

Data availability

The final model and crystallographic data have been deposited into the Protein Data Bank under PDB ID 8FIA (http://identifiers.org/pdb/8FIA). Other raw data are provided in Source Data. Plasmids and other reagents are available upon reasonable request to the corresponding author, Demet Araç.

Expanded View for this article is available online.

Acknowledgments

We thank Dr. Engin Özkan for assistance and discussion on X-ray data collection and structure determination. We also thank the staff at GM/CA. GM/CA@APS has been funded by the National Cancer Institute (ACB-12002) and the National Institute of General Medical Sciences (AGM-12006, P30GM138396). The Eiger 16 M detector at GM/CA-XSD was funded by NIH grant S10 OD012289. Finally, we thank the staff at NE-CAT. This work is based upon research conducted at the Northeastern Collaborative Access Team beamlines, which are funded by the National Institute of General Medical Sciences from the National Institutes of Health (P30 GM124165). The Eiger 16 M detector on the 24-ID-E beam line is funded by a NIH-ORIP HEI grant (S10OD021527). This research used resources of the Advanced Photon Source; a U.S. Department of Energy (DOE) Office of Science User Facility operated for the DOE Office of Science by Argonne National Laboratory under Contract No. DE-AC02-06CH11357. The mass photometry analysis was performed by the Biophysics Core in Research Resources Center of University of Illinois at Chicago. This work was supported by R01GM134035 (to D.A.), R35GM148412 (to D.A.) and F32GM142266 (to S.J.B.).

Author contributions

Jingxian Li: Conceptualization; data curation; formal analysis; validation; investigation; visualization; methodology; project administration; writing – review and editing. **Sumit J Bandekar:** Conceptualization; data curation; formal analysis; funding acquisition; validation; investigation; visualization; methodology; writing – original draft; project administration; writing – review and editing. **Demet Araç:** Conceptualization; resources; formal analysis; supervision; funding acquisition; validation; visualization; methodology; writing – review and editing.

Disclosure and competing interests statement

The authors declare that they have no conflict of interest.

References

Aldahmesh MA, Mohammed JY, Al-Hazzaa S, Alkuraya FS (2012) Homozygous null mutation in ODZ3 causes microphthalmia in humans. *Genet Med* 14: 900 – 904

Alkelai A, Olender T, Haffner-Krausz R, Tsoory MM, Boyko V, Tatarskyy P, Gross-Isseroff R, Milgrom R, Shushan S, Blau I *et al* (2016) A role for TENM1 mutations in congenital general anosmia. *Clin Genet* 90: 211 – 219

Ashkenazy H, Abadi S, Martz E, Chay O, Mayrose I, Pupko T, Ben-Tal N (2016) ConSurf 2016: an improved methodology to estimate and visualize evolutionary conservation in macromolecules. *Nucleic Acids Res* 44: W344 – W350

Bagutti C, Forro G, Ferralli J, Rubin B, Chiquet-Ehrismann R (2003) The intracellular domain of teneurin-2 has a nuclear function and represses zic-1-mediated transcription. *J Cell Sci* 116: 2957 – 2966

Baumgartner S, Wides R (2019) Discovery of teneurins. *Front Neurosci* 13: 1 – 9

Baumgartner S, Martin D, Hagios C, Chiquet-Ehrismann R (1994) tenm, a *Drosophila* gene related to tenascin, is a new pair-rule gene. *EMBO J* 13: 3728 – 3740

Ben-Zur T, Feige E, Motro B, Wides R (2000) The mammalian odz gene family: homologs of a *Drosophila* pair-rule gene with expression implying distinct yet overlapping developmental roles. *Dev Biol* 217: 107 – 120

Berns DS, DeNardo LA, Pederick DT, Luo L (2018) Teneurin-3 controls topographic circuit assembly in the hippocampus. *Nature* 554: 328 – 333

Boucard AA, Maxeiner S, Südhof TC (2014) Latrophilins function as heterophilic cell-adhesion molecules by binding to teneurins: regulation by alternative splicing. *J Biol Chem* 289: 387 – 402

Brasch J, Goodman KM, Noble AJ, Rapp M, Mannepalli S, Bahna F, Dandey VP, Bepler T, Berger B, Maniatis T *et al* (2019) Visualization of clustered protocadherin neuronal self-recognition complexes. *Nature* 569: 280 – 283

Broz DK, Tucker RP, Leachman NT, Chiquet-Ehrismann R (2010) The expression of teneurin-4 in the avian embryo: potential roles in patterning of the limb and nervous system. *Int J Dev Biol* 54: 1507 – 1514

Chassaing N, Ragge N, Plaisancié J, Patat O, Geneviève D, Rivier F, Malrieu-Eliaou C, Hamel C, Kaplan J, Calvas P (2016) Confirmation of TENM3 involvement in autosomal recessive colobomatous microphthalmia. *Am J Med Genet Part A* 170: 1895 – 1898

Dharmaratne N, Glendining KA, Young TR, Tran H, Sawatari A, Leamey CA (2012) Ten-m3 is required for the development of topography in the ipsilateral retinocollicular pathway. *PLoS One* 7: e43083

Dong G, Wearsch PA, Peaper DR, Cresswell P, Reinisch KM (2009) Insights into MHC class I peptide loading from the structure of the tapasin-ERp57 thiol oxidoreductase heterodimer. *Immunity* 30: 21 – 32

Drabikowski K, Trzebiatowska A, Chiquet-Ehrismann R (2005) Ten-1, an essential gene for germ cell development, epidermal morphogenesis, gonad migration, and neuronal pathfinding in *Caenorhabditis elegans*. *Dev Biol* 282: 27 – 38

Emsley P, Lohkamp B, Scott WG, Cowtan K (2010) Features and development of Coot. *Acta Crystallogr Sect D Biol Crystallogr* 66: 486 – 501

Fascetti N, Baumgartner S (2002) Expression of *Drosophila* Ten-a, a dimeric receptor during embryonic development. *Mech Dev* 114: 197 – 200

Feng K, Zhou XH, Oohashi T, Mörgelin M, Lustig A, Hirakawa S, Ninomiya Y, Engel J, Rauch U, Fässler R (2002) All four members of the Ten-m/Odz family of transmembrane proteins form dimers. *J Biol Chem* 277: 26128 – 26135

Goodman KM, Rubinstein R, Thu CA, Bahna F, Mannepalli S, Ahlsén G, Rittenhouse C, Maniatis T, Honig B, Shapiro L (2016) Structural basis of diverse homophilic recognition by clustered α- and β-protocadherins. *Neuron* 90: 709 – 723

Graumann R, Capua GAD, Oyarzún JE, Vásquez MA, Liao C, Brañes JA, Roa I, Casanello P, Corvalán AH, Owen GI *et al* (2017) Expression of teneurins is associated with tumor differentiation and patient survival in ovarian cancer. *PLoS One* 12: e0177244

Hong W, Mosca TJ, Luo L (2012) Teneurins instruct synaptic partner matching in an olfactory map. *Nature* 484: 201 – 207

Hor H, Francescatto L, Bartesaghi L, Ortega-Cubero S, Kousi M, Lorenzo-Betancor O, Jiménez-Jiménez FJ, Gironell A, Clarimón J, Drechse O *et al* (2015) Missense mutations in TENM4, a regulator of axon guidance and central myelination, cause essential tremor. *Hum Mol Genet* 24: 5677 – 5686

Jackson VA, Meijer DH, Carrasquero M, Van Bezouwen LS, Lowe ED, Kleanthous C, Janssen BJC, Seiradake E (2018) Structures of Teneurin

adhesion receptors reveal an ancient fold for cell-cell interaction. *Nat Commun* 9: 1 – 9

Krissinel E, Henrick K (2007) Inference of macromolecular assemblies from crystalline state. *J Mol Biol* 372: 774 – 797

Leamey CA, Sawatari A (2014) The teneurins: new players in the generation of visual topography. *Semin Cell Dev Biol* 35: 173 – 179

Leamey CA, Merlin S, Lattouf P, Sawatari A, Zhou X, Demel N, Glendining KA, Oohashi T, Sur M, Fässler R (2007) Ten_m3 regulates eye-specific patterning in the mammalian visual pathway and is required for binocular vision. *PLoS Biol* 5: 2077 – 2092

Leon K, Cunningham RL, Riback JA, Feldman E, Li J, Sosnick TR, Zhao M, Monk KR, Araç D (2020) Structural basis for adhesion G protein-coupled receptor Gpr126 function. *Nat Commun* 11: 194

Levine A, Bashan-Ahrend A, Budai-Hadrian O, Gartenberg D, Menasherow S, Wides R (1994) odd Oz: a novel *Drosophila* pair rule gene. *Cell* 77: 587 – 598

Levine A, Weiss C, Wides R (1997) Expression of the pair-rule gene odd Oz (odz) in imaginal tissues. *Dev Dyn* 209: 1 – 14

Li J, Shalev-Benami M, Sando R, Jiang X, Kibrom A, Wang J, Leon K, Katanski C, Nazarko O, Lu YC *et al* (2018) Structural basis for Teneurin function in circuit-wiring: a toxin motif at the synapse. *Cell* 173: 735 – 748.e15

Li J, Xie Y, Cornelius S, Jiang X, Sando R, Kordon SP, Pan M, Leon K, Südhof TC, Zhao M *et al* (2020) Alternative splicing controls teneurin-latrophilin interaction and synapse specificity by a shape-shifting mechanism. *Nat Commun* 11: 2140

Liebschner D, Afonine PV, Baker ML, Bunkoczi G, Chen VB, Croll TI, Hintze B, Hung LW, Jain S, McCoy AJ *et al* (2019) Macromolecular structure determination using X-rays, neutrons and electrons: recent developments in Phenix. *Acta Crystallogr Sect D Struct Biol* 75: 861 – 877

Lossie AC, Nakamura H, Thomas SE, Justice MJ (2005) Mutation of l7Rn3 shows that Odz4 is required for mouse gastrulation. *Genetics* 169: 285 – 299

McCoy AJ, Grosse-Kunstleve RW, Adams PD, Winn MD, Storoni LC, Read RJ (2007) Phaser crystallographic software. *J Appl Cryst* 40: 658 – 674

Meijer DH, Frias CP, Beugelink JW, Deurloo YN, Janssen BJC (2022) Teneurin4 dimer structures reveal a calcium-stabilized compact conformation supporting homomeric trans-interactions. *EMBO J* 41: e107505

Mirdita M, Schütze K, Moriwaki Y, Heo L, Ovchinnikov S, Steinegger M (2022) ColabFold: making protein folding accessible to all. *Nat Methods* 19: 679 – 682

Mosca TJ (2015) On the Teneurin track: a new synaptic organization molecule emerges. *Front Cell Neurosci* 9: 204

Mosca TJ, Luo L (2014) Synaptic organization of the *Drosophila* antennal lobe and its regulation by the Teneurins. *Elife* 3: e03726

Mosca TJ, Hong W, Dani VS, Favaloro V, Luo L (2012) Trans-synaptic Teneurin signalling in neuromuscular synapse organization and target choice. *Nature* 484: 237 – 241

Nakamura H, Cook RN, Justice MJ (2013) Mouse Tenm4 is required for mesoderm induction. *BMC Dev Biol* 13: 9

Nunes SM, Ferralli J, Choi K, Brown-Luedi M, Minet AD, Chiquet-Ehrismann R (2005) The intracellular domain of teneurin-1 interacts with MBD1 and CAP/ponsin resulting in subcellular codistribution and translocation to the nuclear matrix. *Exp Cell Res* 305: 122 – 132

Oohashi T, Zhou XH, Feng K, Richter B, Mörgelin M, Perez MT, Su WD, Chiquet-Ehrismann R, Rauch U, Fässler R (1999) Mouse ten-m/odz is a new family of dimeric type II transmembrane proteins expressed in many tissues. *J Cell Biol* 145: 563 – 577

Pederick DT, Lui JH, Gingrich EC, Xu C, Wagner MJ, Liu Y, He Z, Quake SR, Luo L (2021) Reciprocal repulsions instruct the precise assembly of parallel hippocampal networks. *Science* 372: 1068 – 1073

Pei J, Kim BH, Grishin NV (2008) PROMALS3D: a tool for multiple protein sequence and structure alignments. *Nucleic Acids Res* 36: 2295 – 2300

Rubin BP, Tucker RP, Brown-Luedi M, Martin D, Chiquet-Ehrismann R (2002) Teneurin 2 is expressed by the neurons of the thalamofugal visual system in situ and promotes homophilic cell-cell adhesion in vitro. *Development* 129: 4697 – 4705

Sando R, Jiang X, Südhof TC (2019) Latrophilin GPCRs direct synapse specificity by coincident binding of FLRTs and teneurins. *Science* 363: eaav7969

Silva JP, Lelianova VG, Ermolyuk YS, Vysokov N, Hitchen PG, Berninghausen O, Rahman MA, Zangrandi A, Fidalgo S, Tonevitsky AG *et al* (2011) Latrophilin 1 and its endogenous ligand Lasso/teneurin-2 form a high-affinity transsynaptic receptor pair with signaling capabilities. *Proc Natl Acad Sci USA* 108: 12113 – 12118

Südhof TC (2017) Synaptic neurexin complexes: a molecular code for the logic of neural circuits. *Cell* 171: 745 – 769

Talamillo A, Grande L, Ruiz-Ontañon P, Velasquez C, Mollinedo P, Torices S, Sanchez-Gomez P, Aznar A, Esparis-Ogando A, Lopez-Lopez C *et al* (2017) ODZ1 allows glioblastoma to sustain invasiveness through a Myc-dependent transcriptional upregulation of RhoA. *Oncogene* 36: 1733 – 1744

Terwilliger TC (2003) SOLVE and RESOLVE: automated structure solution and density modification. *Methods Enzymol* 374: 22 – 37

Thu CA, Chen WV, Rubinstein R, Chevee M, Wolcott HN, Felsovalyi KO, Tapia JC, Shapiro L, Honig B, Maniatis T (2014) Single-cell identity generated by combinatorial homophilic interactions between α, β, and γ protocadherins. *Cell* 158: 1045 – 1059

del Toro D, Carrasquero-Ordaz MA, Chu A, Ruff T, Shahin M, Jackson VA, Chavent M, Berbeira-Santana M, Seyit-Bremer G, Brignani S *et al* (2020) Structural basis of Teneurin-Latrophilin interaction in repulsive guidance of migrating neurons. *Cell* 180: 323 – 339.e19

Trzebiatowska A, Topf U, Sauder U, Drabikowski K, Chiquet-Ehrismann R (2008) Caenorhabditis elegans teneurin, ten-1, is required for gonadal and pharyngeal basement membrane integrity and acts redundantly with integrin ina-1 and dystroglycan dgn-1. *Mol Biol Cell* 19: 3898 – 3908

Tucker RP (2018) Teneurins: domain architecture, evolutionary origins, and patterns of expression. *Front Neurosci* 12: 1 – 14

Tucker RP, Chiquet-Ehrismann R (2006) Teneurins: a conserved family of transmembrane proteins involved in intercellular signaling during development. *Dev Biol* 290: 237 – 245

Tucker RP, Chiquet-Ehrismann R, Chevron MP, Martin D, Hall RJ, Rubin BP (2001) Teneurin-2 is expressed in tissues that regulate limb and somite pattern formation and is induced in vitro and in situ by FGF8. *Dev Dyn* 220: 27 – 39

Tucker RP, Kenzelmann D, Trzebiatowska A, Chiquet-Ehrismann R (2007) Teneurins: transmembrane proteins with fundamental roles in development. *Int J Biochem Cell Biol* 39: 292 – 297

Tucker RP, Beckmann J, Leachman NT, Schöler J, Chiquet-Ehrismann R (2012) Phylogenetic analysis of the teneurins: conserved features and premetazoan ancestry. *Mol Biol Evol* 29: 1019 – 1029

Williams CJ, Headd JJ, Moriarty NW, Prisant MG, Videau LL, Deis LN, Verma V, Keedy DA, Hintze BJ, Chen VB *et al* (2018) MolProbity: more and better reference data for improved all-atom structure validation. *Protein Sci* 27: 293 – 315

Woelfle R, D'Aquila AL, Lovejoy DA (2016) Teneurins, TCAP, and Latrophilins: roles in the etiology of mood disorders. *Transl Neurosci* 7: 17 – 23

Young TR, Bourke M, Zhou X, Oohashi T, Sawatari A, Fässler R, Leamey CA (2013) Ten-m2 is required for the generation of binocular visual circuits. *J Neurosci* 33: 12490 – 12509

Zhang X, Lin P-Y, Liakath-Ali K, Südhof TC (2022) Teneurins assemble into presynaptic nanoclusters that promote synapse formation via postsynaptic non-teneurin ligands. *Nat Commun* 13: 2297

Zhou XH, Brandau O, Feng K, Oohashi T, Ninomiya Y, Rauch U, Fässler R (2003) The murine Ten-m/Odz genes show distinct but overlapping expression patterns during development and in adult brain. *Gene Expr Patterns* 3: 397 – 405

Ziegler A, Corvalán A, Roa I, Brañes JA, Wollscheid B (2012) Teneurin protein family: an emerging role in human tumorigenesis and drug resistance. *Cancer Lett* 326: 1 – 7

Expanded View Figures

Figure EV1. Structural and sequence differences between TENs.

A–C Structural superimposition of Ten-m (purple) and hTen4 (cyan, used as a stand in for vertebrate TEN structures as a whole) reveal that the overall structure of the TEN superfold is conserved, yet there are differences in specific regions. Inside the barrel, (B): the Ig-like domain takes a different track demarcated by arrows and (C): the portion of the toxin-like domain inside the barrel also follows a different track.

D A β-strand in the β-barrel sterically clashes with the putative binding site of ADGRLs, based on the structure of the hTen2-hADGRL3 complex (PDB 6VHH).

E The all-atom RMSD between representative TEN structures is shown in a table.

F–K The sequence identity of different TEN homologs is compared using the full-length sequence, (F) and broken up individually by domain (G–K).

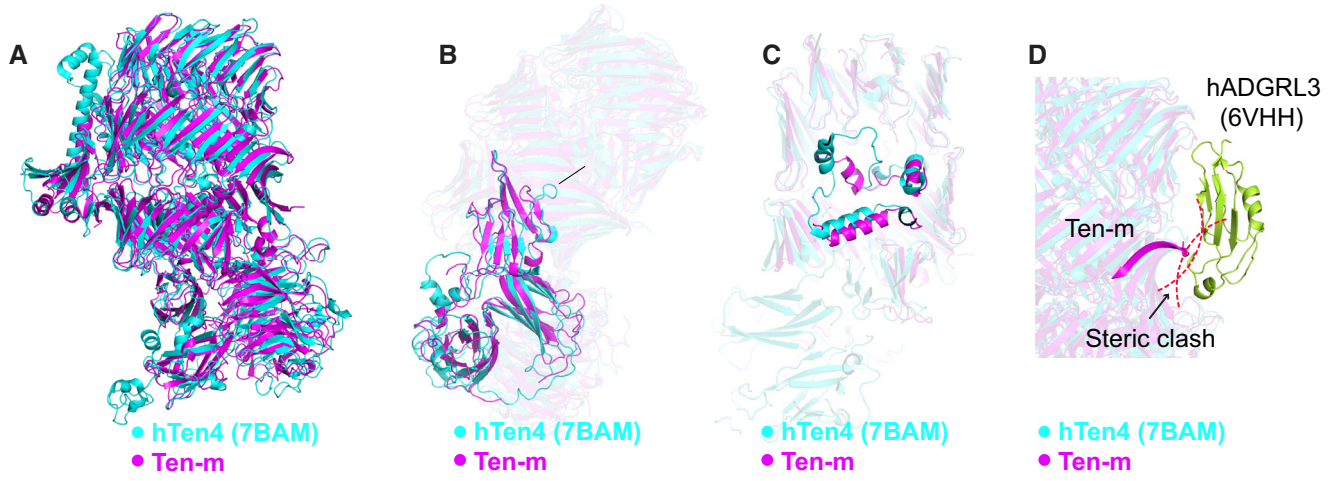

E

	Ten-m	hTen4	ggTen2	hTen2	mTen3
Ten-m	0	5.9	5.8	5.7	5.1
hTen4	5.9	0	2.5	3.1	2.5
ggTen2	5.8	2.5	0	2.0	1.9
hTen2	5.7	3.1	2.0	0	2.4
mTen3	5.1	2.5	1.9	2.4	0

all-atom RMSD (Å)

F

	Ten-m	Ten-a	ceTen-1	zfTen2	ggTen2	mTen2	hTen2
Ten-m	100	50	27	34	35	35	35
Ten-a	50	100	29	40	40	41	41
ceTen-1	27	29	100	27	27	27	27
zfTen2	34	40	27	100	77	78	78
ggTen2	35	40	27	77	100	92	93
mTen2	35	41	27	78	92	100	98
hTen2	35	41	27	78	93	98	100

full length sequence identity (%)

G

	Ten-m	Ten-a	ceTen-1	zfTen2	ggTen2	mTen2	hTen2
Ten-m	100	57	42	49	51	53	51
Ten-a	57	100	39	50	44	45	44
ceTen-1	42	39	100	48	37	36	37
zfTen2	49	50	48	100	88	88	91
ggTen2	51	44	37	88	100	95	97
mTen2	53	45	36	88	95	100	96
hTen2	51	44	37	91	97	96	100

TTR sequence identity (%)

H

	Ten-m	Ten-a	ceTen-1	zfTen2	ggTen2	mTen2	hTen2
Ten-m	100	50	30	43	40	41	40
Ten-a	50	100	27	40	41	41	42
ceTen-1	30	27	100	33	31	31	30
zfTen2	43	40	33	100	77	77	77
ggTen2	40	41	31	77	100	91	93
mTen2	41	41	31	77	91	100	97
hTen2	40	42	30	77	93	97	100

Ig-like sequence identity (%)

I

	Ten-m	Ten-a	ceTen-1	zfTen2	ggTen2	mTen2	hTen2
Ten-m	100	50	33	41	42	43	43
Ten-a	50	100	31	39	40	40	40
ceTen-1	33	31	100	33	32	32	32
zfTen2	41	39	33	100	87	86	86
ggTen2	42	40	32	87	100	96	97
mTen2	43	40	32	86	96	100	98
hTen2	43	40	32	86	97	98	100

β-propeller sequence identity (%)

J

	Ten-m	Ten-a	ceTen-1	zfTen2	ggTen2	mTen2	hTen2
Ten-m	100	32	23	28	29	29	29
Ten-a	32	100	23	27	29	29	29
ceTen-1	23	23	100	23	22	23	23
zfTen2	28	27	23	100	78	79	79
ggTen2	29	29	22	78	100	95	95
mTen2	29	29	23	79	95	100	99
hTen2	29	29	23	79	95	99	100

β-barrel sequence identity (%)

K

	Ten-m	Ten-a	ceTen-1	zfTen2	ggTen2	mTen2	hTen2
Ten-m	100	28	22	28	24	27	27
Ten-a	28	100	20	33	30	28	28
ceTen-1	22	20	100	32	28	28	28
zfTen2	28	33	32	100	67	69	70
ggTen2	24	30	28	67	100	90	91
mTen2	27	28	28	69	90	100	99
hTen2	27	28	28	70	91	99	100

toxin-like sequence identity (%)

Figure EV1.

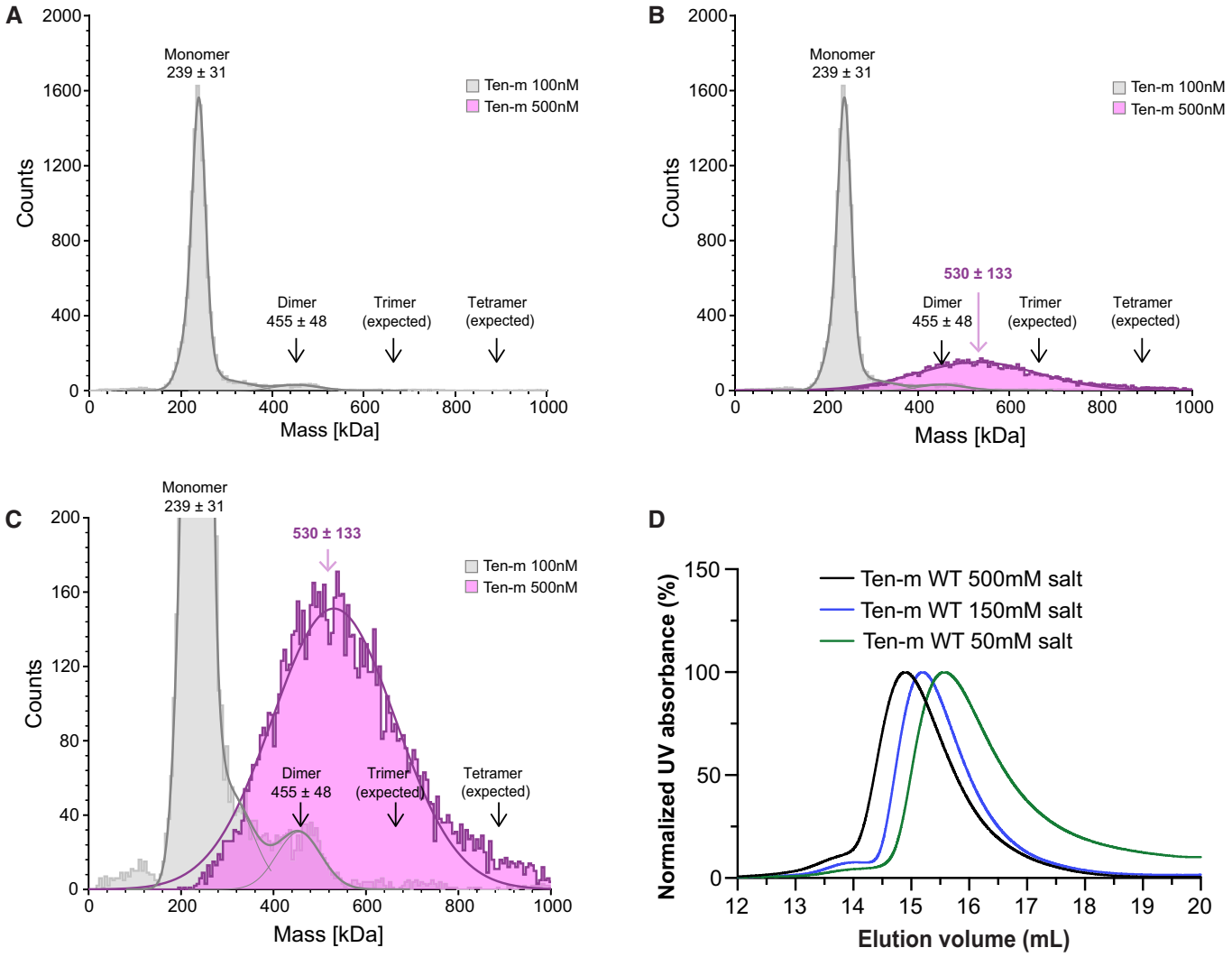

Figure EV2. Further biophysical studies on Ten-m self-association using mass photometry and size exclusion chromatography.

A–C Mass photometry shows an increase in oligomer proportion at higher concentrations. Mass photometry curves, molecular counts vs. mass, shown with 100 nM final Ten-m concentration in gray and 500 nM final concentration in pink. Various zooms in of the Y-axis are shown to show detail on the high concentration plot. The expected molecular mass of the monomer is ~ 222 kDa, dimer is ~ 444 kDa, trimer is ~ 666 kDa, and tetramer is ~ 888 kDa, and they are highlighted using arrows. Counts are observed consistent with the presence of higher order species.

D SEC chromatograms with A_{280} versus elution volume plotted show that increasing salt (NaCl) concentrations shift the protein toward an earlier elution volume. Mass photometry and SEC experiments were performed once, $N = 1$.

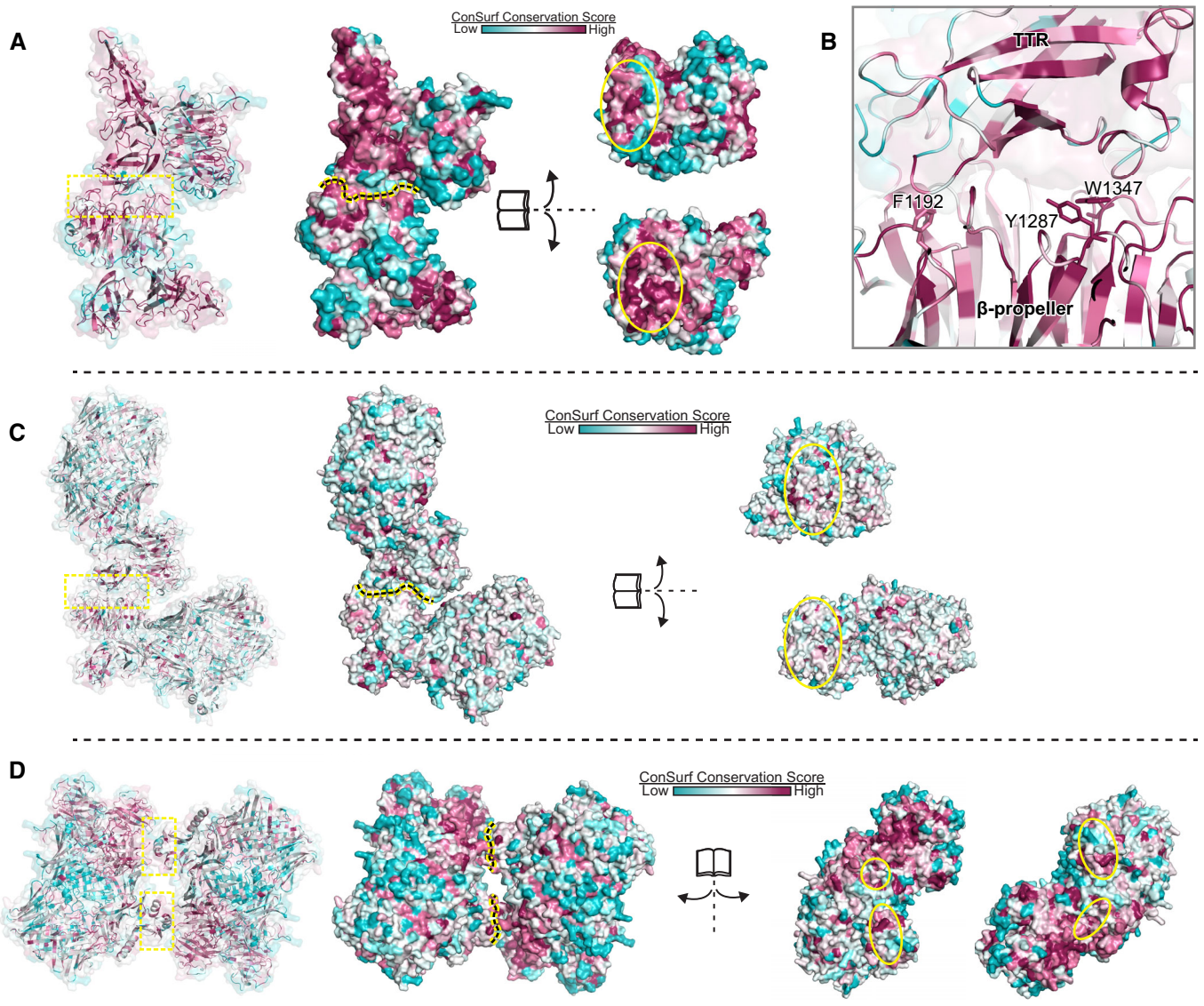

Figure EV3. Sequence conservation of the Ten-m self-association interface.

The ConSurf server was used to assess surface conservations of Ten-m and make comparisons with other TENs. The conservation score is plotted onto a surface representation of each structure. Purple indicates high conservation, cyan indicates low conservation, and white indicates intermediate conservation.

A The ConSurf server was used to generate a sequence alignment of Ten-m using homologs with greater than 35% sequence identity. The conservation score is plotted onto a surface representation of the self-association interface with the TTR, Ig-like, and β-propeller shown. Yellow dotted lines and ovals enclose the Ten-m surface used for self-association and show that it is largely composed of conserved residues.

B A close-up view shows that the residues which break the binding interface when mutated, including F1192, Y1287, and W1347 are strongly conserved.

C A sequence alignment of Ten-m using homologs across animals was plotted onto the Ten-m self-association interface.

D The ConSurf server is used to generate a sequence alignment of Ten-m using homologs with greater than 35% sequence identity. The conservation score is plotted onto a surface representation of Ten-m arranged in the Ten4 β-barrel/toxin-like dimer. Yellow dotted lines and ovals enclose the Ten4 dimer surface and show that it is not strongly conserved in arthropods.

Figure EV4. The EGF-dimer leads to many possible scenarios for Ten-m self-association.

Many possibilities are present and they can also mix and match each other.

A If Ten-m self-associates in *cis*, there are two reasonable possibilities for this: the interface could form between two superfolds part of the same EGF-dimer (left), or between two superfolds protruding from different EGF dimers (right).

B If the interface forms in *trans*, a "parallel" situation could occur (left) where a set of superfolds protruding from the same EGF dimer is occupied by another completed set, or an asymmetric situation (right) where the one superfold of each opposing EGF dimer is occupied in the Ten-m self-association interface, and the other two superfolds are free to form similar *trans* association with other EGF dimers, or *cis* self-associated Ten-m molecules.

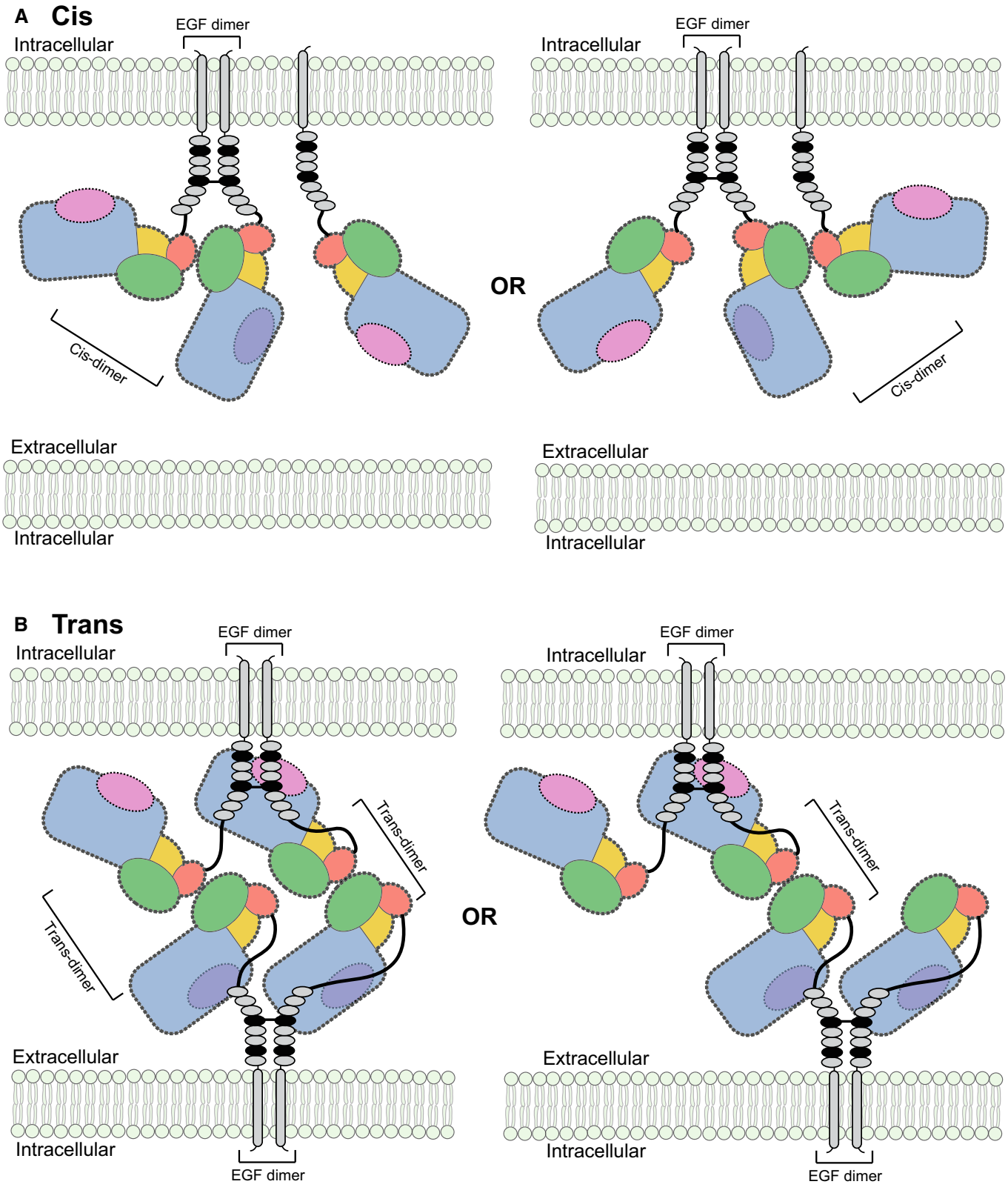

Figure EV4.

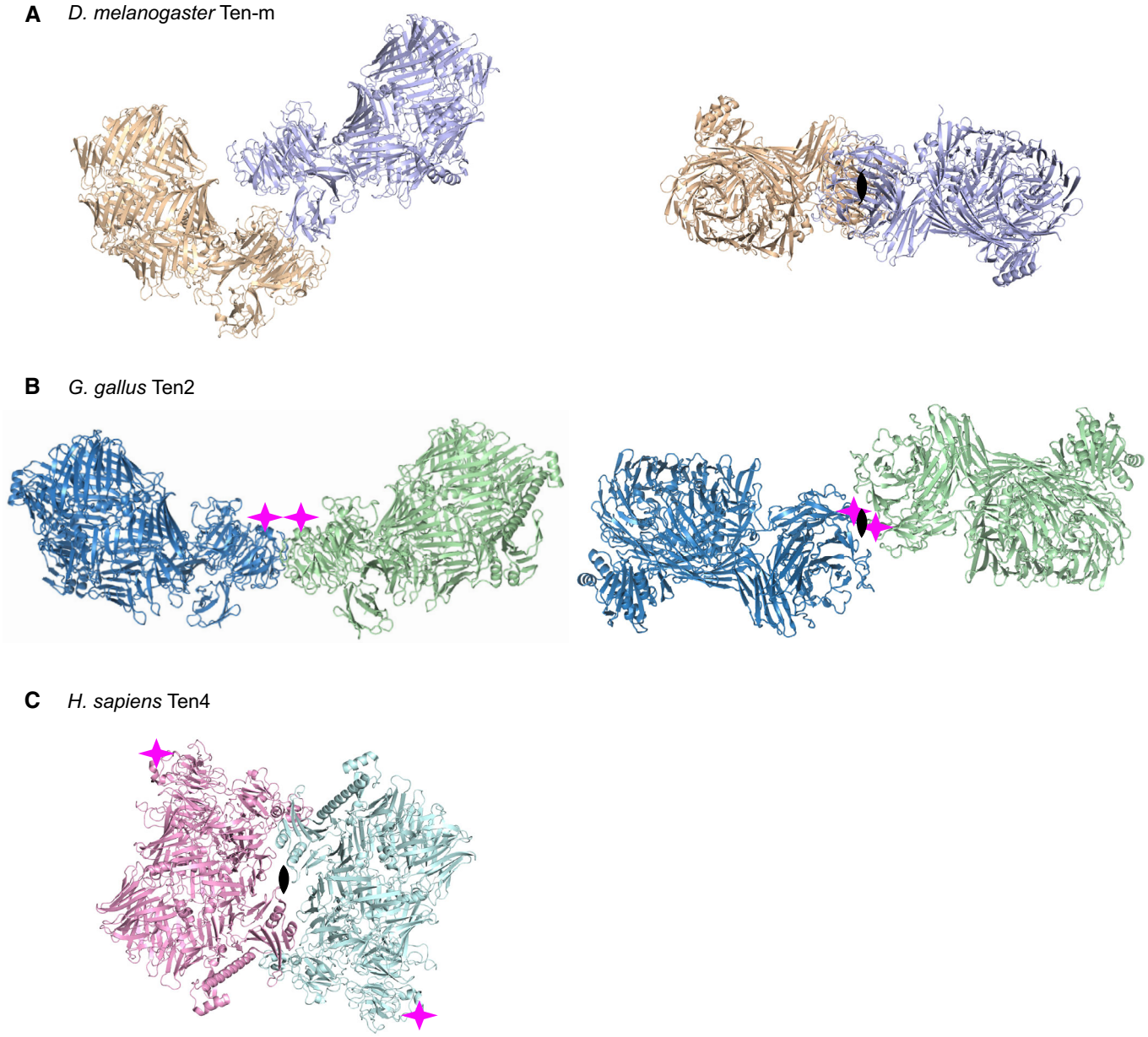

Figure EV5. Comparing available TEN oligomer structures.

PyMol was used to generate cartoon representations of TEN oligomerization.

A The Ten-m self-association interface (this manuscript, PDB 8FIA).

B The ggTen2 dimer (PDB 6FB3). Individual monomers are shown in contrasting colors. The vertebrate-specific splice site in the β-propeller domain is shown as a pink star.

C the hTen4 dimer (PDB 7BAM). Symmetry operators which generate each presented interface are shown, with a 2_1 screw axis for Ten-m self-association, and twofold axes for ggTen2 and hTen4 dimers.

Appendix for: "The structure of fly Teneurin-m reveals an asymmetric self-assembly that allows expansion into zippers"

Jingxian Li[#], Sumit J. Bandekar[#], and Demet Araç[*]

Department of Biochemistry and Molecular Biology, University of Chicago, Chicago, IL, 60637, USA.

The University of Chicago Neuroscience Institute, University of Chicago, Chicago, IL, 60637, USA.

Institute for Biophysical Dynamics, University of Chicago, Chicago, IL, 60637, USA

# - These authors contributed equally to this study.

*Corresponding author: Demet Araç, arac@uchicago.edu

Table of Contents:

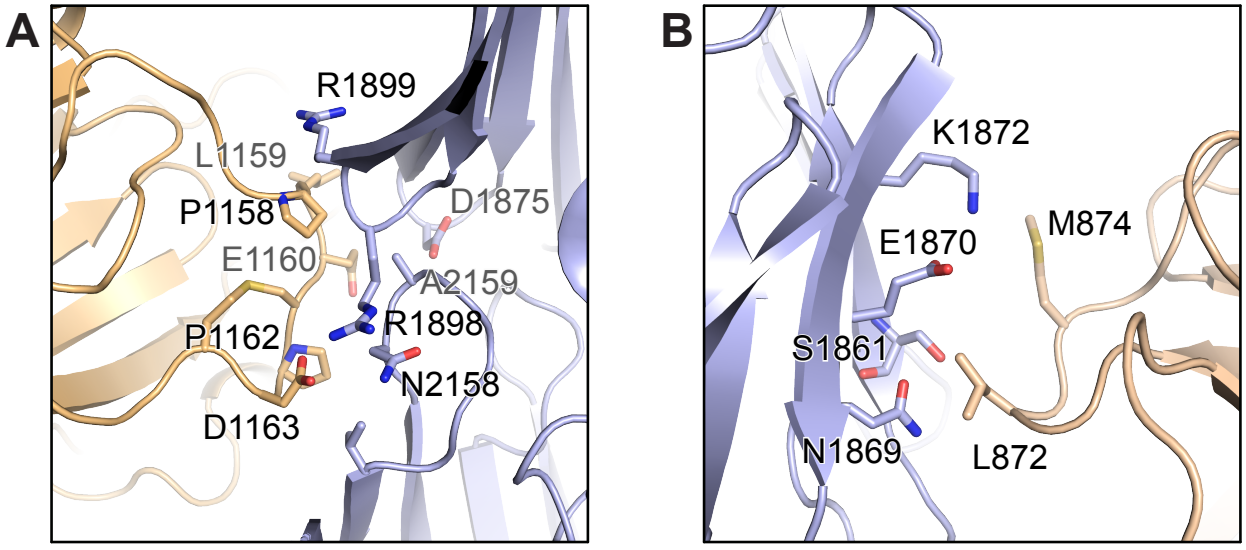

Appendix Figure S1: Crystal contacts within the Ten-m structure. Using PDB ePISA, major contact interfaces were identified within the Ten-m crystal packing. The largest interface is the one depicted in the manuscript as the putative Ten-m self-association interface. The next two largest interfaces are depicted. Neither interface is large or well conserved, so they were not studied further.

A. 420 Å^2 is buried from solvent in this interface.

B. 150 Å^2 is buried from solvent in this interface.

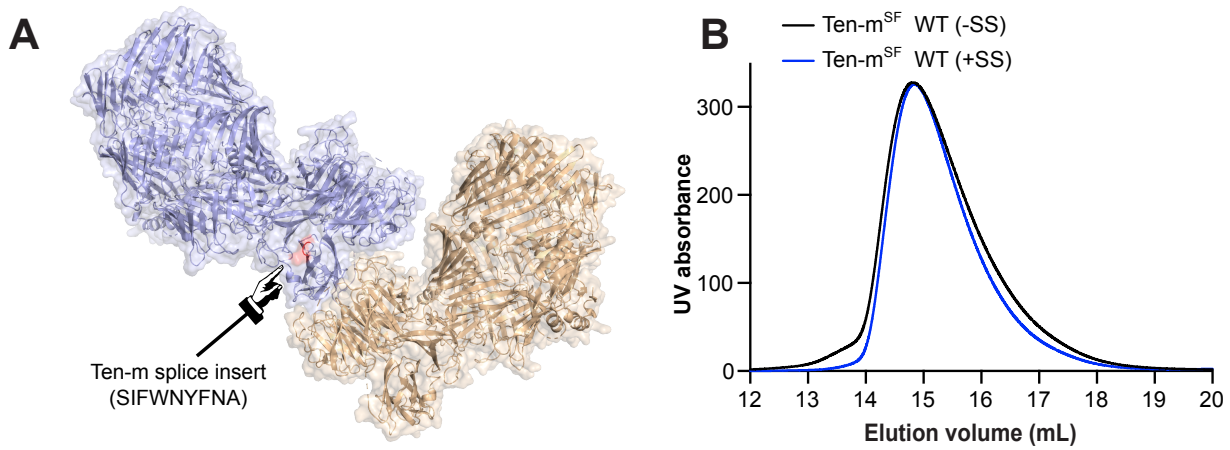

Appendix Figure S2: The presence of an alternatively spliced sequence in the TTR domain does not disrupt the observed Ten-m dimer in solution.

A. The Ten-m dimer is shown in a cartoon representation. Each monomer is colored differently, and the loop region which the alternatively spliced sequence (SIFWNYFNA) would insert into is highlighted in pink, with a pointer emphasizing its location.

B. SEC chromatograms with A_{280} plotted vs. elution volume show that the presence of the alternatively spliced sequence does not shift the elution volume of Ten-m. SEC experiments were performed with N=1.